TECHNISCHE UNIVERSITÄT WIEN
Vienna University of Technology

Diplomarbeit

Studies on the structural determination of coordination compounds using ESI MS and MALDI MS

ausgeführt zum Zwecke der Erlangung des akademischen Grades eines

Diplom-Ingenieurs

unter der Leitung von

Prof. DI Dr. Karl Kirchner

Priv.Doz. Mag. Dr. Ernst Pittenauer

eingereicht an der Technischen Universität Wien

Fakultät für Technische Chemie

von

Fleissner Sarah

9841 Winklern

Wien, Februar 2020

_____

Sarah Fleissner

TECHNISCHE UNIVERSITÄT WIEN
Vienna University of Technology

Ich habe zur Kenntnis genommen, dass ich zur Drucklegung meiner Arbeit unter der Bezeichnung

Diplomarbeit

nur mit Bewilligung der Prüfungskommission berechtigt bin.

Ich erkläre weiters Eides statt, dass ich meine Diplomarbeit nach den anerkannten Grundsätzen für wissenschaftliche Abhandlungen selbstständig ausgeführt habe und alle verwendeten Hilfsmittel, insbesondere die zugrunde gelegte Literatur, genannt habe.

Weiters erkläre ich, dass ich dieses Diplomarbeitsthema bisher weder im In- noch Ausland (einer Beurteilerin/einem Beurteiler zur Begutachtung) in irgendeiner Form als Prüfungsarbeit vorgelegt habe und dass diese Arbeit mit der vom Begutachter beurteilten Arbeit übereinstimmt.

Wien, Februar 2020

_____

Sarah Fleissner

Abstract

The areas of application of coordination compounds range from their use in industry as catalysts to medicine and pharmacy. In order to establish newly synthesized complexes, first of all a complete characterization of these compounds is necessary. One of the most important analytical techniques used for this purpose are IR, NMR and EPR spectroscopy. Although each of these techniques is essential and indispensable, they only offer the possibility of complete clarification of a substance in combination with mass spectrometry.

This thesis deals with the analysis of coordination compounds using MALDI MS. The selection of the analytes was made with a view to cover the broadest possible spectrum of transition metal elements and ligand systems. By variation of MALDI matrices, solvent mixtures and measurement parameters, the optimal preparations for a successful analysis were taken individually for each complex. The resulting data were compared with the already established ionization technique ESI MS.

All coordination compounds selected in the course of this work were successfully analyzed with MALDI MS. It was also possible to determine the accurate mass of each compound with a mass deviation of < 5 ppm of the theoretical value.

Kurzfassung

Die Anwendungsbereiche von Koordinationsverbindungen reichen von ihrem Einsatz in der Industrie als Katalysatoren bis hin zur Medizin und Pharmazie. Um neu synthetisierte Komplexe etablieren zu können ist in erster Linie eine vollständige Charakterisierung dieser erforderlich. Eine der wichtigsten Analysetechniken die hierbei in Verwendung treten sind die IR-, NMR-, als auch EPR-Spektroskopie. Obgleich jede der genannten Techniken essenziell und unabdingbar ist, bieten sie nur in Kombination mit der Massenspektrometrie die Möglichkeit der vollständigen Aufklärung eines Stoffes.

Diese Arbeit beschäftigt sich mit der Analyse von Koordinationsverbindungen mittels MALDI MS. Die Auswahl der Analyten erfolgte im Hinblick darauf ein möglichst breites Spektrum an Elementen der Übergangsmetalle, sowie Ligandensysteme zu bedienen. Durch Variation von MALDI Matrices, Lösemittelgemischen und Messparametern wurden für jeden Komplex individuell die optimalen Voraussetzungen für eine erfolgreiche Analyse getroffen. Die daraus generierten Daten wurden mit der bereits etablierten Ionisationstechnik ESI MS vergleichend gegenübergestellt.

Die im Zuge dieser Arbeit ausgewählten Koordinationsverbindungen konnten erfolgreich mit MALDI MS analysiert werden. Auch war es möglich die akkurate Masse jeder Verbindung mit einer Massenabweichung von < 5 ppm des theoretischen Wertes zu bestimmen.

Danksagung

Diese Arbeit kann im metaphorischen Sinne als wichtiger Meilenstein eines Weges betrachtet werden. Aus diesem Grund bietet sich mir hier die Möglichkeit all jenen Menschen zu danken, die mich auf den unterschiedlichsten Abschnitten begleitet haben.

Zu Beginn möchte ich mich bei Prof. Karl Kirchner bedanken, ohne dessen Betreuung und Unterstützung die hier vorliegende Arbeit nicht möglich gewesen wäre. Außerdem möchte ich mich an dieser Stelle noch einmal ausdrücklich für sein aufrichtiges Interesse an meiner Forschungsarbeit bedanken.

Ebenso möchte ich Prof. Ernst Pittenauer meinen größten Dank aussprechen. Nicht nur für das ausgezeichnete Betreuungsverhältnis, sondern auch für seine Offenheit für neue Ideen und Vorschläge. Ich bin wirklich dankbar dafür, dass er seine ausgeprägten Fachkenntnisse in umfangreichen Gesprächen mit mir geteilt hat.

Weiters möchte ich mich bei allen aktuellen, sowie ehemaligen Mitgliedern der Forschungsgruppen von Karl Kirchner und Wolfgang Linert, insbesondere bei Jan Pecak und Stefan Weber, für ihren wissenschaftlichen Beitrag zu meiner Arbeit bedanken. Die Erinnerungen an die abseits aller seriösen Wissenschaften gemeinsam verbrachten Abende werde ich stets mit einem Schmunzeln in Erinnerung behalten.

Auch möchte ich mich bei Victoria Dorrer, Edita Rados und Philipp Crepaz aus der Forschungsgruppe von Günter Allmaier für den fachlichen Austausch und die amüsanten Gespräche während der Arbeitspausen bedanken.

Ein weiterer Dank ergeht an das gesamte Personal der Institute E163 und E164, wo ich besonders Herbert Hutter, Peter Weinberger und Michael Luger namentlich nicht unerwähnt lassen möchte.

Aufrichtiger Dank gilt auch meinen Freunden, allen voran Adrian Strasser, Theresia Baumgartner und Philip Piller. Danke für eure Unterstützung und für die schönen, unvergesslichen Erlebnisse!

Aus dem familiären Kreis möchte ich mich vor allem bei meinen Eltern bedanken, die es mir durch ihre finanzielle Unterstützung ermöglicht haben, dieses Studium zu absolvieren. Ein großer Dank gilt auch meiner Schwester Hannah und meinen Großeltern.

Zum Schluss möchte ich mich noch aus tiefsten Herzen bei Dir, Jan, bedanken. Du warst in dieser aufregenden Zeit stets der Ruhepol, der so genannte „Fels in der Brandung“, auf dessen Unterstützung ich immer zählen konnte.

[Non si può predire] nulla: nulla di sicuro, nulla di probabile, nulla di onesto

Primo Levi (1919-1987)

Table of Contents

1 Introduction

Coordination compounds serve a wide range of applications, for example as catalysts in industry and in medicine/pharmacology. One of the first known coordination compounds is the potassium trichloro(ethylene)platinate(II), also called Zeise's salt. The compound was discovered around 1831 by the Danish scientist William Christopher Zeise.[1] The first organometallic complex to gain importance as a drug was arsphenamine, also known as Salvarsan, which was introduced by Paul Ehrlich, the founder of modern antibacterial chemotherapy.[2] This substance was used for the treatment of syphilis.[3] Over the past decades, research on coordination compounds has been intensified and gained in importance, especially in the industrial sector.[4] It should also be mentioned that these substances often show a very high reactivity and are often sensitive to both oxidation and hydrolysis. Therefore, in many cases it is necessary to carry out sample preparation (starting with filling and dissolving the complex) under exclusion of air. This can be achieved by using the Schlenk technique or by working in a glovebox. Analytical methods for the characterization of newly synthesized complexes include IR, NMR, EPR spectroscopy, single crystal diffraction and mass spectrometry. The most commonly used ionization technique for mass spectrometric analysis is electrospray ionization (ESI). Despite some advantages offered by ESI MS (e.g. fast and easy sample preparation), the analysis of neutral coordination compounds is still a challenge.[5] The analysis of such analytes using MALDI MS is an area that has received very little research so far.[6–8] This thesis deals with the development of a method to successfully analyze coordination compounds using (HR)MALDI MS. A major advantage of MALDI MS compared to ESI MS is the possibility of analyzing neutral complexes and spatially resolved detection of the analyte. This makes MALDI MS also suitable for imaging experiments on tissue sections.

2 Theoretical aspects

2.1 Coordination compounds

2.1.1 Definition

Coordination chemistry is a part of inorganic chemistry, which deals in particular with complex compounds. A complex consists of a central atom and ligands. A complexing reaction can be described as an acid-base reaction according to Lewis, with the central atom acting as electron pair acceptor and the ligand as electron pair donor.

A special branch of coordination chemistry is organometallic chemistry. An organometallic compound is defined as such if at least one metal-to-carbon bond exists (e.g. BuLi, PhMgBr).[9]

2.1.2 Area of application

As already mentioned in the introduction, complexes are often used as catalysts in industry. The high reactivity and also selectivity of these compounds is of importance here. Well-known representatives in this field are the Grubbs catalysts, which are used in olefin metathesis.[10] In 2005, scientists were awarded the Nobel Prize for their research on these catalysts and for elucidating the reaction mechanism. Representative for the application of coordination compounds in the field of medicine is cis-diammine dichloridoplatinum, colloquially also known as "cisplatin". It belongs to the drug class of cytostatics and is used to treat various cancers. The effect is that the substance inhibits DNA replication by cross-linking two adjacent guanine bases of a DNA strand.[11]

2.1.3 Handling and use

Although a high reactivity of the complexes is desired, this is often accompanied by sensitivity to oxidation and hydrolysis. For this reason the correct handling of this substance class is of immense importance. The Schlenk technique offers the possibility to work under exclusion of oxygen and water.[12] For particularly sensitive compound, however, it may be necessary to work in a glove box.

2.2 Mass spectrometry

2.2.1 General information

Mass spectrometry is a powerful analytical technique for the analysis of atoms and molecules. The basic principle is to transfer a substance into the gas phase, ionize it and then separate it on the basis of its mass-to-charge ratio. Nowadays, many different mass spectrometers are used, which differ in their ionization principles, analyzers and detector systems. However, the basic structure is the same for all different instrumentations. As shown in Figure 1, a mass spectrometer consists of the following components: A sample inlet system, which is under atmospheric pressure or vacuum. As the name suggests, the ionization source is used to ionize the sample molecules, which are then separated in the analyzer based on their mass-to-charge ratio. Afterwards the ions are detected. The signals of the ions are converted into electrical signals according to their abundance. Finally, the detector signals are transmitted to a data processing system.[13]

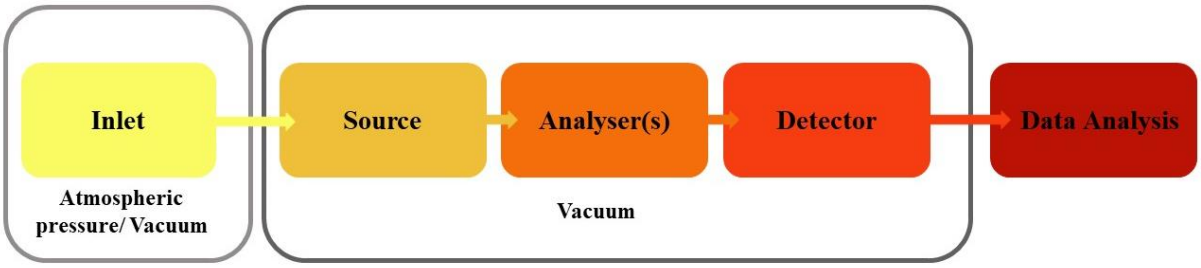

Figure 1: General construction of a mass spectrometer

2.2.2 Ionization techniques

When selecting a suitable ionization technique, the chemical and physical properties of the analyte must always be taken into account. To facilitate the selection, a distinction can be made between the following two large groups: “Hard ionization techniques” and “soft ionization techniques”. The decisive factor in which group an ionization technique belongs is the amount of energy transferred during ionization. The "hard ionization technique", as it is called, can lead to a strong fragmentation of the analyte molecules due to a higher energy input. An example of a hard ionization technique is electron ionization (EI). In contrast, the "soft ionization technique" mainly detects the ionized molecule species. The group of soft ionization techniques includes electrospray ionization (ESI) and matrix-assisted laser desorption/ionization (MALDI).[14] Subsequently, the ionization techniques ESI and MALDI will be discussed in more detail, as these have also been used in the course of the work.

2.2.2.1 ESI

John B. Fenn, Kurt Wüttrich and Koichi Tanaka received the 2002 Nobel Prize for "the development of methods for the identification and structural analysis of biological macromolecules", with Fenn's work focusing on the development of electrospray

ionization. In order to carry out ionization by means of electrospray, it is necessary that the sample is in the liquid state. ESI can be obtained by applying an electric field and the flow of a liquid substance through a capillary. Figure 2 illustrates the principle of electrospray ionization.

In the course of electrospray ionization, the liquid sample is passed through a metal capillary. An electric field is generated between the tip of the capillary and the counter electrode by applying a potential difference. As a result, charge is transferred to the liquid surface at the tip of the capillary (Taylor cone), from which highly charged drops are formed. These droplets emerge from the capillary as fine aerosols. To support the evaporation of the solvent, either a neutral carrier gas such as nitrogen or a heated capillary is used. In the course of solvent evaporation, the radius of the charged droplets becomes smaller, which means that the density of the electric field at its surface is increased. If the Rayleigh limit, which states that gas-charged droplets can only absorb a certain number of the same charge, is exceeded, a so-called "Coulomb explosion" occurs. The droplets disintegrate into smaller droplets due to repulsion of the same charge. How these actually free charges can develop will be described with the ion evaporation model or with the charge residue model. The entire process takes place under atmospheric pressure.[15,16]

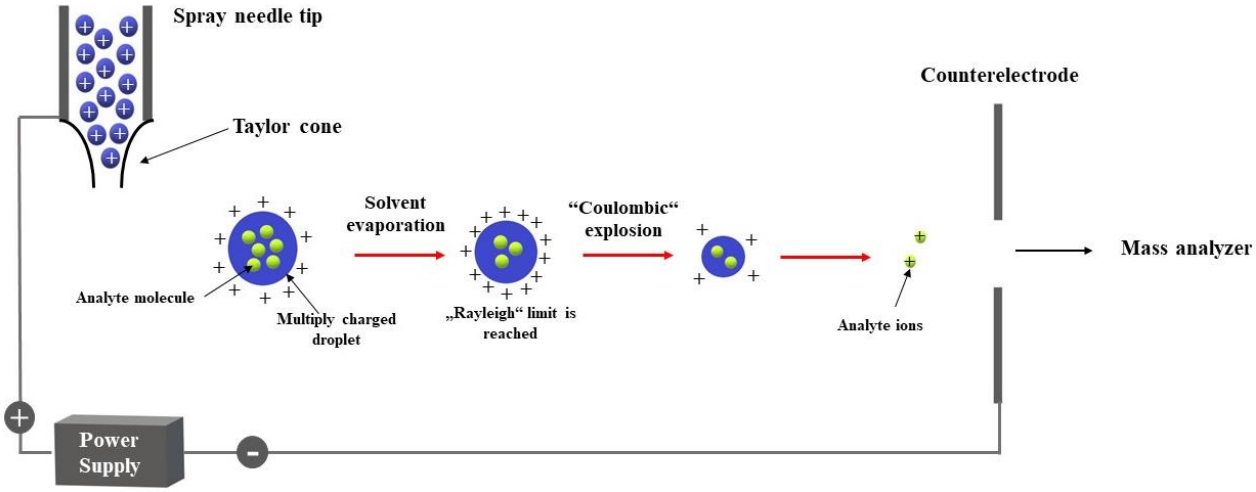

Figure 2: Principle of electrospray ionization process

ESI is a powerful ionization technique that can be applied to a wide range of different analytes. A big advantage is the high sensitivity, but also the possibility of coupling with a chromatography unit (e.g. HPLC). ESI can generate positive as well as negative ions, which can be $[M+H]^+$, $[M+nH]^{n+}$ or $[M-H]^-$ or $[M-nH]^{n-}$. Another aspect of this technique is the formation of adductions ($[M+Na]^+$, $[M+K]^+$) by the addition or presence of corresponding salts.[17]

2.2.2.2 MALDI

The principle of MALDI was first introduced by Franz Hillenkamp and Michael Karas in 1988. Almost simultaneously, Koichi Tanaka was working on a similar procedure for which he was awarded the Nobel Prize in 2002 (see chapter 2.2.2.1).

The matrix thus designated is an organic molecule present as a solid which is primarily dissolved in a suitable solvent. Furthermore, the matrix solution is combined with the sample and the solvent is evaporated as a result. This leads to co-crystallization of the analyte and matrix molecules. The analytes are now isolated from each other and embedded in the matrix. The solid solution is ablated by the input of pulsed laser energy. The desorption and ionization process takes place almost simultaneously. The exact sequence of ionization has not been fully clarified.[18] One possible proposal is ionization according to the cluster ionization mechanism, which assumes that the analytes retain the charge state from the solution. The ions are then accelerated in the electric field and fed into the analyzer, which in the case of MALDI is very often a time-of-flight analyzer. The principle of MALDI is illustrated in Figure 3.[14,19]

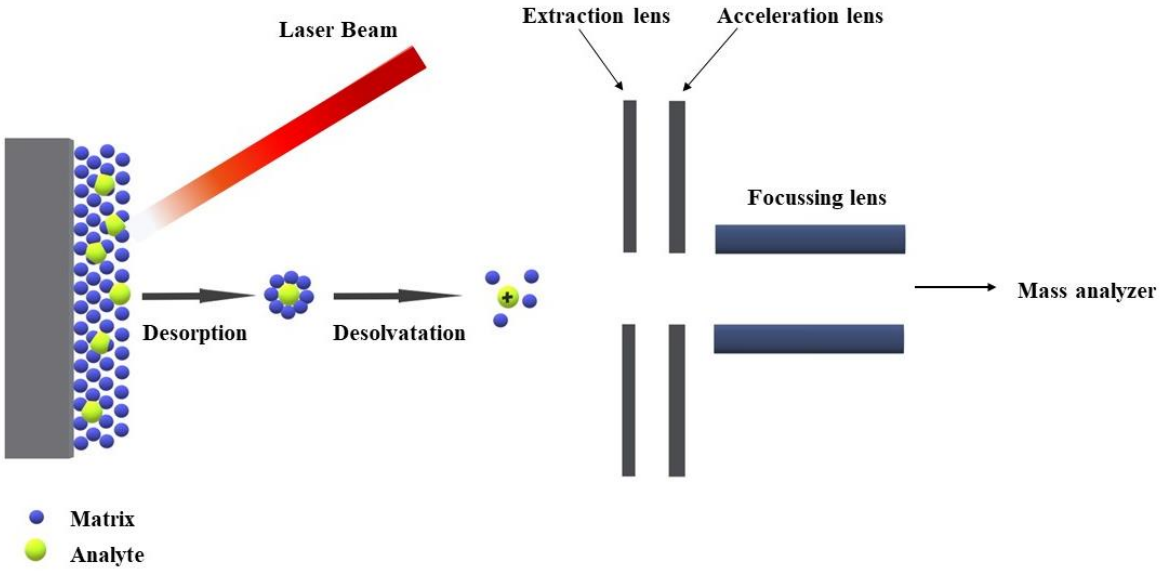

Figure 3: Principle of the matrix-assisted-laser/ionization process

MALDI MS is a sensitive technique which allows very high molecular mass measurements (up to 200-300 kDa, with special detector up to 1 MDa).[20]

2.2.3 Mass analyzers

In the mass analyzer, the ions are separated according to their mass-to-charge ratio under vacuum conditions. There are many types of mass analyzers which are based on different separation principles. Roughly speaking, analyzers can be divided into two large groups - analyzers that allow only certain masses to be transmitted at a certain time and analyzers that allow simultaneous transmission for all ions. The first group includes magnetic sector field and quadrupole instruments. Examples of analyzers in the second group are time-of-flight, but also ion and orbitrap instruments. Important parameters of a mass spectrometer are resolution, mass accuracy, transmittance and mass limitations.[21] The resolution is defined by the extent to which a distinction can be made between two ions with mass to charge ratios close to each other. A common indication of the resolving power of mass spectrometers today is the R_{FWHM} (full width at half maximum). Thus the

resolution is defined by the quotient of the ion mass and the width of a peak in the spectrum at half peak maximum (equation (2.1)).[22]

$$R_{FWHM} = \frac{m}{\Delta m} \tag{2.1}$$

R_{FWHM}	resolving power
m	m/z ratio [Th]
Δm	full width at half maximum [Th]

The level of resolution varies from analyzer to analyzer. An FT-ICR (Fourier-transform ion cyclotron resonance) mass analyzer with R_{FWHM} = 500 000 can achieve the highest resolving power, while the values for the quadrupole are significantly lower (R_{FWHM} = 2000). With a TOF mass analyzer, a resolving power of 20 000 (reflectron mode) or 5000 (linear mode) can be realized. These values refer to the assumption of a m/z of 1000. The mass accuracy is a value which calculates the difference between the measured m/z value and the theoretical one. This is usually expressed in ppm (parts per million). Transmission consists of the quotient of the number of ions arriving at the detector and the number of ions entering the source. The mass limitation indicates up to which m/z ratio a substance can be detected. It is given in the unit Thomson (Th). The mass spectrometer with the highest mass range is the TOF in linear mode (1 000 000 Th for singly charged ions).[21] Since the quadrupole and time-of-flight mass analyzers were used in the course of this work, they will be discussed in more detail below.

2.2.3.1 Quadrupol mass analyzer

In 1953 the principle of the quadrupole was first described by the scientists Paul and Steinwegen. The functional principle of a quadrupole analyzer is based on the stability of

the trajectory of the ions in an oscillating electric field. Figure 4 shows a graphical representation of the separation principle of a quadrupole mass analyzer.[23]

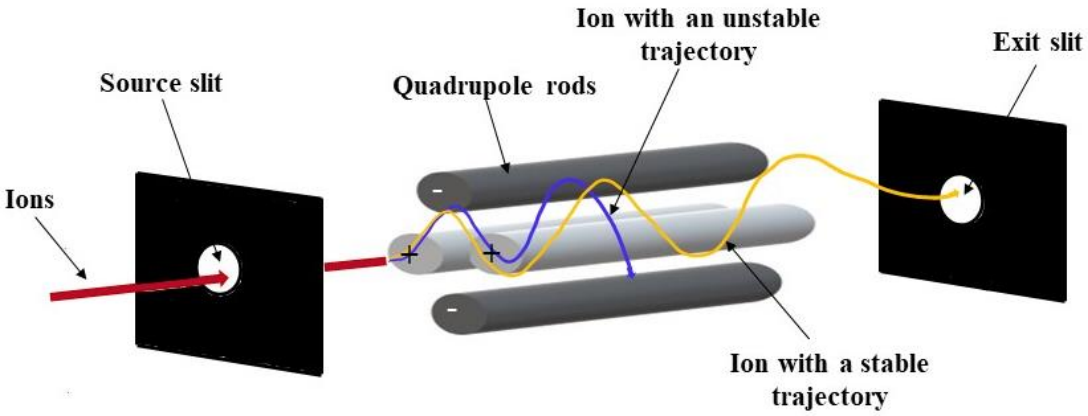

Figure 4: Schematics of a quadrupole mass analyzer

It consists of four rod electrodes which are exactly parallel to the ion path. A static and oscillating voltage is applied between the rods:

$$\phi = U - V \cdot \cos(2\pi\nu t) \tag{2.2}$$

ϕ potential applied to the rods [V]

U direct potential [V]

V "zero to peak" amplitude of the RF voltage [V]

ν frequency of the radio frequency field [Hz]

By fixing the voltages U and V, only ions with a certain m/z ratio can pass through the analyzer. Since the quadrupole mass analyzer is one of the cheapest, it is also very often used. Another advantage is the fast analysis time. The limiting factor of the quadrupole mass analyzer is the relatively low resolution compared to others.[21]

2.2.3.2 Time of flight mass analyzer

In 1955 Wiley and McLaren first published the concept of a linear time-of-flight analyzer. Today, there are two different types of TOF analyzers: LTOF (linear time-of-flight) and RTOF (reflectron time-of-flight). Nowadays, both types are built into one device, whereby the respective measuring mode can be selected via the instrument control software. The principle of time-of-flight instruments is based on the different flight times of the previously accelerated ions when drifting along the field-free flight tube.[24] Figure 5 schematically shows a linear time-of-flight analyzer.

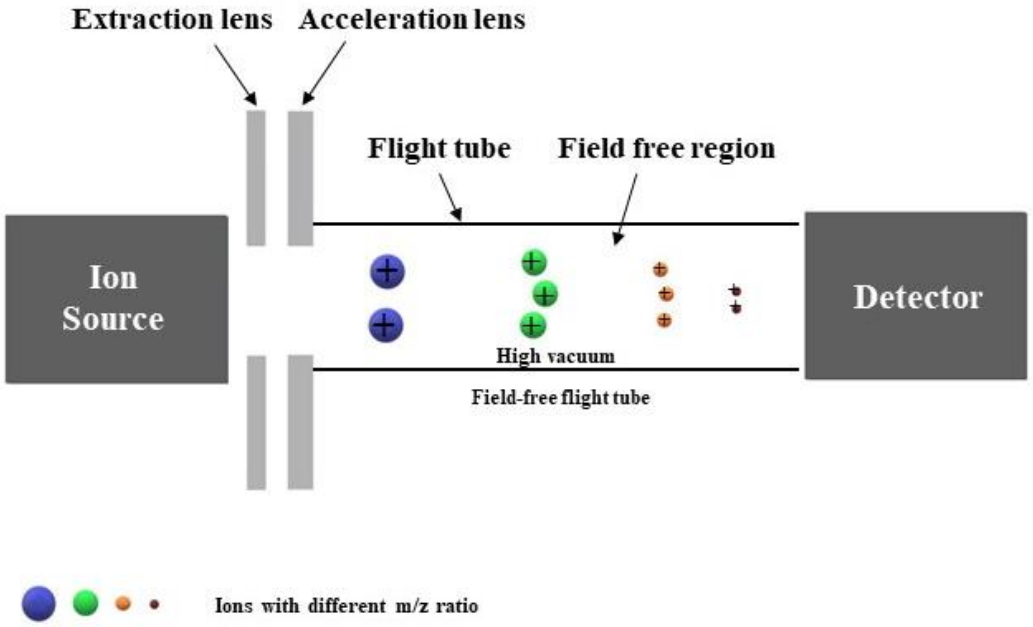

Figure 5: Graphical representation of a linear time-of-flight analyzer

Assuming E_{Kin} (kinetic energy) = E_{el} (electric potential energy) equations 2.3 and 2.4 follow:

$$v = \left(\frac{2 \cdot z \cdot e \cdot V_s}{m}\right)^{1/2} \tag{2.3}$$

$$t = \frac{L}{v} \tag{2.4}$$

v velocity [m/s]

m mass [kg]

z charge

e elementary charge [C]

V_s acceleration potential [V]

t time [s]

L drift path [m]

The equations show that if the other parameters are equal, the mass of the ion is decisive for the time it has passed through the flying tube. Theoretically, ions with the same m/z ratio should have the same kinetic energy after leaving the source. In reality, however, this is not the case due to initial kinetic energy spread of particular ions. For this reason the use of the RTOF proves to be meaningful, since it corrects the differences in the energy distribution (i.e. energy focusing). Ions with a higher kinetic energy penetrate deeper into the reflector field, while ions with a lower kinetic energy are already deflected beforehand.[21] As a result, the ions with the same mass/charge ratio arrive at the detector at the same time.

2.2.4 Detectors

2.2.4.1 Electron multiplier

In mass spectrometry, two different classes of electron multiplier (EM) are frequently used: Discrete dynode and continuous dynode electron multipliers. A schematic representation of an electron multiplier with discrete dynode is shown in Figure 6. The figure shows that several dynodes with decreasing negative voltage are connected in succession. The first dynode acts as a conversion dynode, which converts ions into electrons. The generated electrons are accelerated to the next dynode, where secondary electrons are emitted after hitting the surface of the dynode. This kind of chain reaction

continues until the electrons arrive at the last dynode, which is at ground potential. Electric current can be measured.

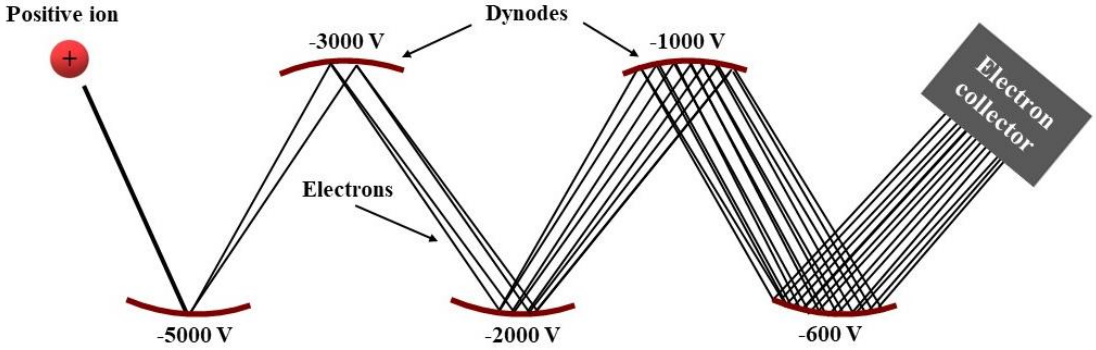

Figure 6: Schematic representation of an electron multiplier with discrete dynode

With the second type, the continuous dynode electron multiplier (CDEM), shown in Figure 7, the number of dynodes is reduced to a single continuous dynode. It has the shape of a funnel made of glass and coated with a semi-conducting layer. There is an electrical resistance on the walls and a voltage is applied between the two ends of the tube, creating a continuous acceleration field. The electrons pass through the tube, where they emit secondary electrons when hitting the wall. At the end, the electron cascade meets the detector output, where a signal can be measured as electric current. Since the process is repeated several times, 10^5 to 10^6 electrons can be generated at the end.

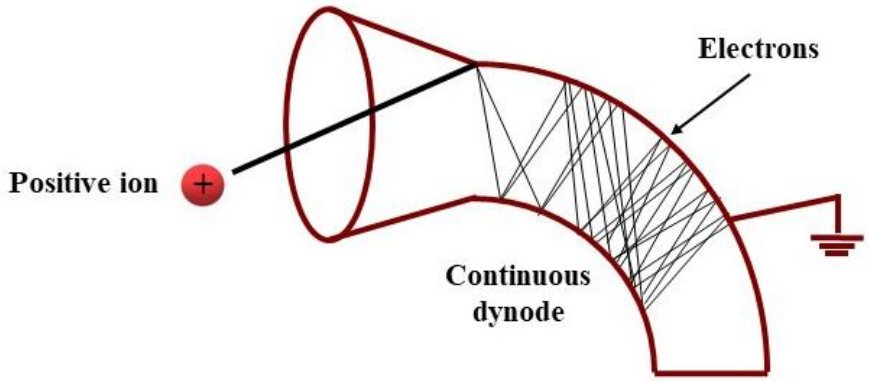

Figure 7: Schematic representation of an electron multiplier with continuous dynode

Another CDEM type is the microchannel plate (see Figure 8).

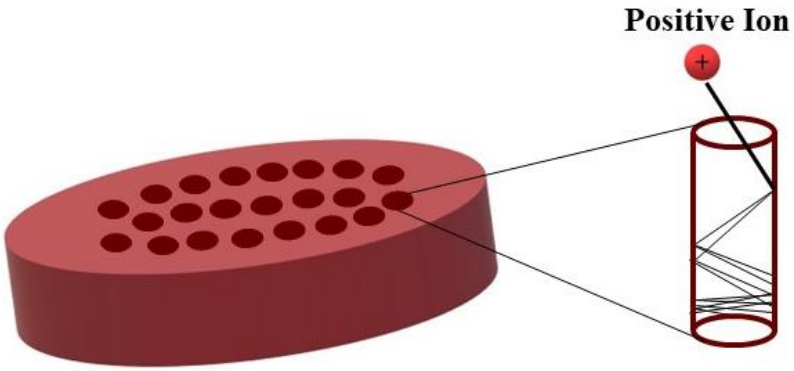

Figure 8: Graphical representation of a multichannel plate

This is a metal plate to which an acceleration voltage is applied. There are many small channels in the plate, which are coated with a semiconductor material. The channels are shifted by an angle from the normal plane of the plate, which causes the electrons to hit the channel wall several times. Each individual channel behaves like a channel electron multiplier. Usually several MCPs are connected in succession. Thus a number of electrons of up to 10^8 can be achieved. The advantage of the microchannel plate is the fast response time and the ability of single ion counting. MCPs can be damaged by high ion intensity,

which is a disadvantage of this type of detector. Furthermore, the dynamic range is narrow.[21]

2.3 Sample preparation for MALDI MS

MALDI MS is a powerful technique to measure a large number of different analytes. However, this can only be achieved by selecting the appropriate matrix and an adequate sample preparation. In the following subchapters, both matrix selection and different types of sample preparation are discussed in more detail.

2.3.1 Matrix selection

Matrix selection must always be individually adapted to the analyte. It is optional to select a matrix, which strongly absorbs the energy at the respective laser wavelength. The MALDI MS mainly uses two different laser types: N_2 lasers (λ= 337 nm) and Nd:YAG lasers (λ=355 nm). Furthermore, matrices can be divided into different groups, which are listed in Table 1.

Table 1: Molar absorption of the laser energy of a Nd:YAG laser (355 nm) for different matrix classes[6]

Matrix type	Matrix	ε_M [$M^{-1}cm^{-1}$]	Laser type
Acidic matrices	αCHCA	23.500	Nd: YAG (355nm)
	SA	5.100	
	DHB	400	
	DT	2.100	
Broensted (Lewis) base matrices	TTP	33.500	
	DCTB	31.410	

Charge-transfer matrices	Pyrene	2.240
	Anthracene	5.250

The matrices listed in this table are the most frequently used in the course of MALDI mass spectrometry. Acidic matrices such as α-CHCA, DHB and SA are often used for the determination of peptides, or even proteins. Broensted (Lewis) base matrices are particularly well suited for the analysis of polymers and inorganic materials. Also charge-transfer matrices such as pyrene and anthracene are suitable for these analytes, in combination with a N_2 laser, but the molar absorption of the laser energy for the Nd:YAG laser is very low.[6]

2.3.2 Matrix application for MALDI MS experiments

In this chapter different forms of sample preparation for MALDI MS experiments are presented. Among the best known methods are the so-called *dried-droplet method*, the *thin-layer method*, but also the *sandwich method*.

Concerning the *dried-droplet method*, a drop of the sample solution is applied to a suitable target and then mixed with a drop of the matrix solution directly on the target. Another variant of this method is to mix matrix and sample solution in advance and then apply it on the target. Finally, the drops are dried either in the air or under a stream of nitrogen.

For the *thin-layer method*, a drop of the matrix solution is applied to the target and dried completely. In the second step, a drop of the sample solution is applied directly to the already dried matrix solution.

The *sandwich method* can be regarded as an extension of the *thin-layer method*. First the matrix solution is applied and dried. Then the sample solution is applied and dried. At the end another drop of matrix solution is added on top.[25]

3 Experimental Part

3.1 Instrumentation

3.1.1 ultrafleXtreme™

The ultrafleXtreme™ is a MALDI TOF/RTOF mass spectrometer from Bruker. This is a high-vacuum MALDI TOF mass spectrometer, where the source is under high-vacuum ($2.1 \cdot 10^{-6}$ mbar). The instrument is equipped with a 2 kHz smartbeam II laser system with a near-rectangular beam profile. The laser is a frequency tripled Nd:YAG laser at a wavelength of 355 nm. The mass spectrometer is a time-of-flight spectrometer, which can be operated in both linear and (dual stage) reflectron mode.

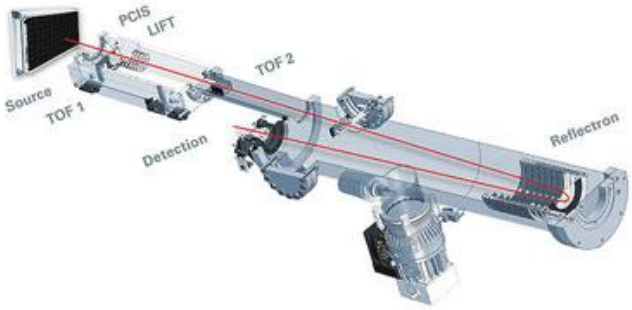

Figure 9: left: ultraflextreme™ (Bruker); right: Setup of the ultrafleXtreme™ [30]

3.1.2 Synapt™ G2 HDMS

The Synapt™ G2 HDMS is a MALDI QRTOF mass spectrometer from Waters. In contrast to the ultrafleXtreme™ described above, this is an intermediate pressure MALDI QRTOF mass spectrometer, where the ion source is operated under a pressure of $2.1 \cdot 10^{-1}$ mbar. The instrument is equipped with a 1 kHz Nd:YAG laser, which has a Gaussian

laser beam profile. It consists of a quadrupole, a so-called Triwave™ section (for ion mobility measurements) and an oa-TOF (orthogonal acceleration) mass analyzer.

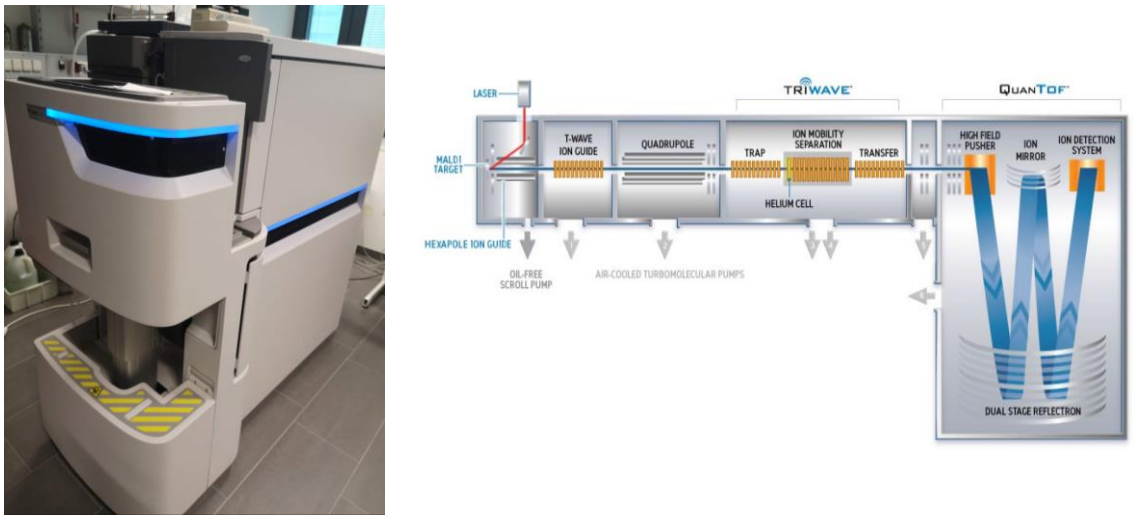

Figure 10: left: Synapt G2 HDMS (Waters); right: Setup of the Synapt™ G2 HDMS[31]

3.1.3 Agilent 6545 QTOF

The Agilent 6545 QTOF is a mass spectrometer from Agilent, which is also combinable with a LC unit. The instrument is optionally equipped with a dual electrospray ionization or a so-called MMI (combination of ESI and APCI) source. It consists of a quadrupole, an rf-only quadrupole collision cell and an (dual stage) reflectron time-of-flight mass analyzer.

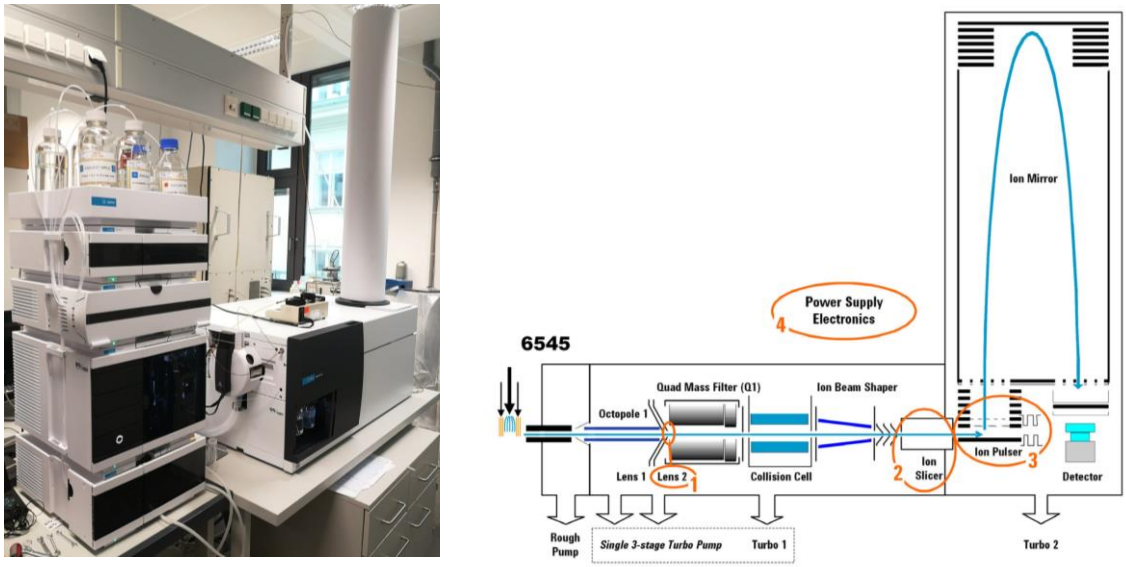

Figure 11: left: Agilent 6545 (Agilent); right: Setup of the Agilent 6545 QTOF system[32]

3.2 Material and methods

3.2.1 Chemicals

Table 2: Chemicals used in the course of the thesis

Chemical	Purity	Company
1,2-Dichloropropane	≥ 99.8 %	Fluka (St. Gallen, CH)
Acetone	≥ 99.5 %	Sigma Aldrich (St.Louis, USA)
Acetonitrile	EMSURE®, p.A	Merck (Billerica, USA)
Chloroform	EMSURE®, p.A	Merck (Billerica, USA)
DCTB	≥ 99.0 %	Merck (Billerica, USA)
Dichloromethane	≥ 99.8 %	VWR (Radnor, USA)
Ethanol	EMSURE®, p.A	Merck (Billerica, USA)
Methanol	≥ 99.9 %	Honeywell (Morristown, USA)
Red phosphorus	≥ 97.0 %	Sigma-Aldrich (St.Louis, USA)

Sodium bromide	≥ 99.5 %	TCI Chemicals (Tokyo, Japan)
Sodium chloride	p.A	Merck (Billerica, USA)
TTP	> 98.0 %	TCI Chemicals (Tokyo, Japan)

3.2.2 General instrumentation and disposable materials

Table 3: General instrumentation and disposable materials used in the course of the thesis

Instrument/Material	**Company**
Analytical Balance Extend	Sartorius (Göttingen, DE)
Disposable Antistatic Microspatulas	VWR (Radnor, USA)
Eppendorf Research Pipette 0.1-2.5 µL	Eppendorf (Hamburg, DE)
Eppendorf Research Pipette 100-1000 µL	Eppendorf (Hamburg, DE)
Eppendorf Research Pipette 20-200 µL	Eppendorf (Hamburg, DE)
epT.I.P.S Reloads 0.1-10 µL Eppendorf tips	Eppendorf (Hamburg, DE)
epT.I.P.S Reloads 100-1000 µL Eppendorf tips	Eppendorf (Hamburg, DE)
epT.I.P.S Reloads 20-200 µL Eppendorf tips	Eppendorf (Hamburg, DE)
Millipore Simplicity UV	Merck (Billerica, USA)
Safe-Lock Tubes 0.5 mL	Eppendorf (Hamburg, DE)
Safe-Lock Tubes 1.5 mL	Eppendorf (Hamburg, DE)
Syringe Pump	KD Scientific (Holliston, USA)
Ultrasonic Bath	Sonorex (Berlin, DE)
Vortex Mixer 524	Labinco (Breda, NL)

3.3 Coordination compounds

In the course of the analysis of complexes, 18 different coordination compounds were investigated. These were synthesized in the research group "Organometallic Chemistry and Catalysis".[26–28] All investigated coordination compounds are listed in Figure 12. The notation for the complexes can be obtained from Table 4.

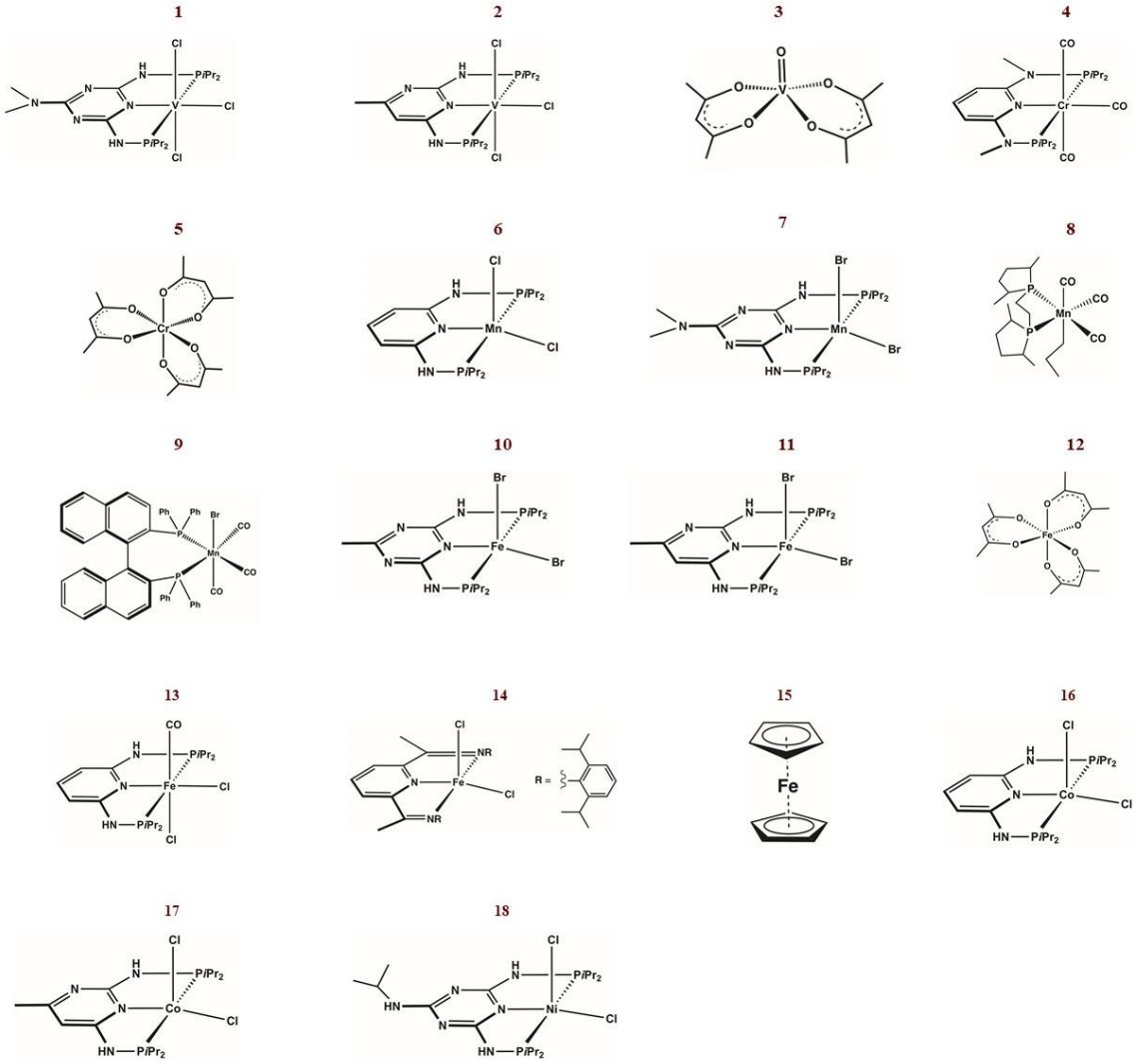

Figure 12: Coordination compounds selected in the course of this work

Table 4: Notation of coordination compounds

Number	Sample code / Notation
1	[V(Triaz^{NMe2}-*i*Pr)Cl_3]
2	[V(Pym^{Me}-*i*Pr)Cl_3]
3	[V(acac)2(O)]
4	[Cr(PNP^{NMe}-*i*Pr)$(CO)_3$]
5	[Cr$(acac)_3$]
6	[Mn(PNP^{NH}-*i*Pr)Cl_2]
7	[Mn(Triaz^{NMe2}-*i*Pr)Br_2]
8	[Mn(me-bpe)$(CO)_3(C_3H_7)$]
9	[Mn(BINAP)$(CO)_3$Br]
10	[Fe(Triaz^{Me}-*i*Pr)Br_2]
11	[Fe(Pym^{Me}-*i*Pr)Br_2]
12	[Fe$(acac)_3$]
13	[Fe(PNP^{NH}-*i*Pr)(CO)Cl_2]
14	[Fe(NNN-PDI)Cl_2]
15	Cp_2Fe
16	[Co(PNP^{NH}-*i*Pr)Cl_2]
17	[Co(Pym^{Me}-*i*Pr)Cl_2]
18	[Ni(Triaz^{NiPr}-*i*Pr)Cl_2]

3.3.1 Sample preparation for analysis by MALDI MS

The sample preparation for the investigated coordination compounds are shown in Figure 13 below. Two different matrices with four combinations of solvent mixtures were tested (see Table 5).

Table 5: Selected matrices and solvent mixtures

Matrix	Solvent 1	Solvent 2	Vol. ratio [v/v]
DCTB	Acetonitrile	Dichloromethane	1:1
	Methanol	Chloroform	
	Methanol	Dichloromethane	
	Dichloropropane	Chloroform	
TTP	Acetonitrile	Dichloromethane	
	Methanol	Chloroform	
	Methanol	Dichloromethane	
	Dichloropropane	Chloroform	

Regarding sample preparation, the *dried-droplet method* was utilized. Initially the matrix was mixed with the respective solvent mixture and dissolved. The concentration of the matrix was 10 mg/mL. In addition, 0.6 mg/mL of sodium chloride or sodium bromide was added to each matrix solution. The selection of the sodium salt depended on the ligands of the investigated complexes. Sodium chloride or sodium bromide was added to compounds in which a chlorine or bromine atom is present as ligand (particularly for neutral compounds). In coordination compounds without halides, sodium chloride was added. The matrix solution was then applied directly to the solid sample, resulting in an analyte concentration of 10 mg/mL. The sample was then dissolved and an aliquot of this solution (0.7 µL) was applied onto a MALDI MS target.

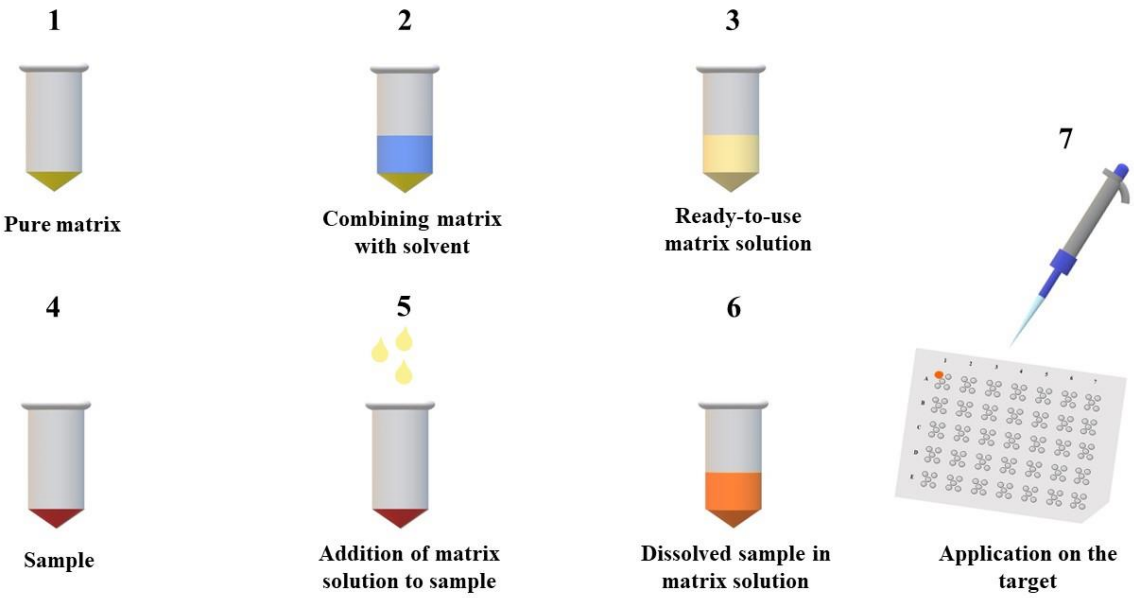

Figure 13: Graphical representation of sample preparation for coordination compounds

3.3.2 Sample preparation for analysis by ESI MS

In the course of ESI MS measurements, the samples were dissolved in the respective solvent mixtures from Table 5. This resulted in a sample concentration of 0.1 mg/mL. Here, 0.6 mg/mL of a sodium salt was also added to the analyte solutions according to the selection criterion described in 3.3.1. The sample solution was introduced into the instrument by direct injection using a Hamilton syringe with a pump.

3.3.3 MALDI MS parameters

In the following chapter the measurement parameters of the MALDI MS experiments are presented. Two different instruments were used for the measurements: the Synapt^{TM} G2 HDMS, an intermediate pressure MALDI QTOF, which also allows high-resolution spectra and the determination of the accurate mass, and the high vacuum MALDI TOF/RTOF ultrafleXtreme^{TM}.

ultrafleXtreme ™

After optimizing the parameters, the experiments with the ultrafleXtreme™ were carried out under the measurement conditions listed in Table 6.

Table 6: Measurement parameters of the MALDI MS experiments with the ultrafleXtreme™

Parameter	**Value**
Ion mode	Positive
TOF geometry	Reflectron
Laser fluence	40 %
Frequency	1 kHz
Shots per spectrum	1000

Synapt™ G2 HDMS

Table 7 gives an overview of the optimized settings of Synapt™ G2 HDMS measurements. After each sample a lock mass correction was performed by measuring a certain m/z of the calibrant and correcting with the theoretical value. The Lock mass was selected to be as close as possible to the m/z value of the analyte to ensure that the deviation from the theoretical m/z value is as small as possible.

Table 7: Measurement parameters of the MALDI MS experiments with the Synapt™ G2 HDMS

Parameter	**Value**
Ion mode	Positive
Laser fluence	320 [a.u.]
Frequency	1 kHz
Scan rate	1 s per scan
Measurement duration	90 s
Acquisition mode	Spiral

3.3.4 ESI MS parameters

During ESI MS measurements with the Agilent 6545 QTOF, the parameters in Table 8 proved to be the optimal instrument settings. It is important to note that the temperature was varied individually for each analyte to ensure optimal ionization conditions and to prevent thermal decomposition. In this case, the lock mass correction takes place directly - this means that the lock mass consisting of four selected calibration peaks in a mass range between m/z 100-1000 was measured together with the sample at the same time.

Table 8: Measurement parameters of the ESI MS experiments with the Agilent 6545 QTOF

Parameter	**Value**
Ion mode	Positive
Ion source temperature	220-240°C
Nebulizer gas pressure	60 psi
Dry gas flow rate	8 L/min

4 Results and Discussion

In this chapter the results of this work are presented and discussed. It should be noted that all MALDI TOF instruments have been calibrated with red phosphorus prior to measurement.[29] For ESI measurements, the instrument was calibrated with an Agilent LCMS tuning mix.

The calculated spectra which are presented in the discussion of the results were performed with the Isopro v3.0 software. Spectra of the ultrafleXtreme™ were processed with the flexAnalysis v3.4 software (Bruker). For the evaluation of the Synapt™ G2 HDMS measurement data the MassLynx v4.1 software from Waters was used. Data from measurements performed with the Agilent 6545 Q-TOF were processed using Agilent's MassHunter Workstation Qualitative Analysis 10.0 software.

4.1 General information

The effects of different matrices, solvent mixtures, ionization methods and instruments were examined in the analysis of the coordination compounds listed in chapter 3.3. All spectra listed in the following chapters were measured in positive ion mode.

4.1.1 Comparison of different matrices

As already mentioned, all coordination compounds were analyzed with two different matrices in the course of this work. Figure 14 shows a comparison between the two matrices (DCTB and TTP) using complex **No.6** as an example. The results show that both spectra are almost identical. This is not only true for example complex **No.6**, but can be applied to all measured coordination compounds. There is also no difference in terms of ionization - the exact same molecular ions can be detected with the same intensity for both matrices.

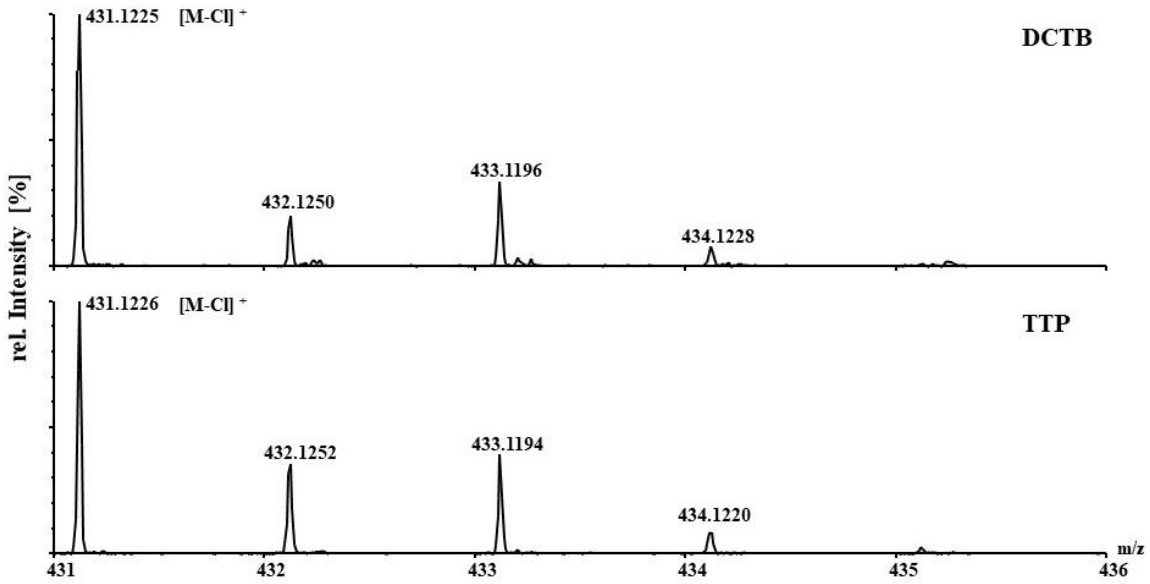

Figure 14: Comparison between different matrices (DCTB, TTP) of complex **No.6**; Instrument: Synapt^{TM} G2 HDMS

4.1.2 Comparison of different solvent mixtures

In this chapter the effect of the use of different solvent mixtures on the analysis of the coordination compounds is presented. This is discussed here using the example of complex **No. 6**, a coordination compound with manganese as the metal center. Figure 15 shows spectra of complex **No. 6**, which were prepared with different solvent mixtures. It can be seen that the monoisotopic peak $[M\text{-}Cl]^+$ and the characteristic isotope pattern of the compound is not visible in all the spectra listed. Specifically, the compound can only be detected in the solvent mixtures of MeOH/TCM and DCP/TCM. The reason for this is that the complex is not soluble in the remaining solvent mixtures or is not present as a stable molecule in the solution. Manganese compounds in particular are generally known to be poorly soluble in various solvents. For this reason, this is a good example to illustrate the relevance for the correct choice of a solvent.

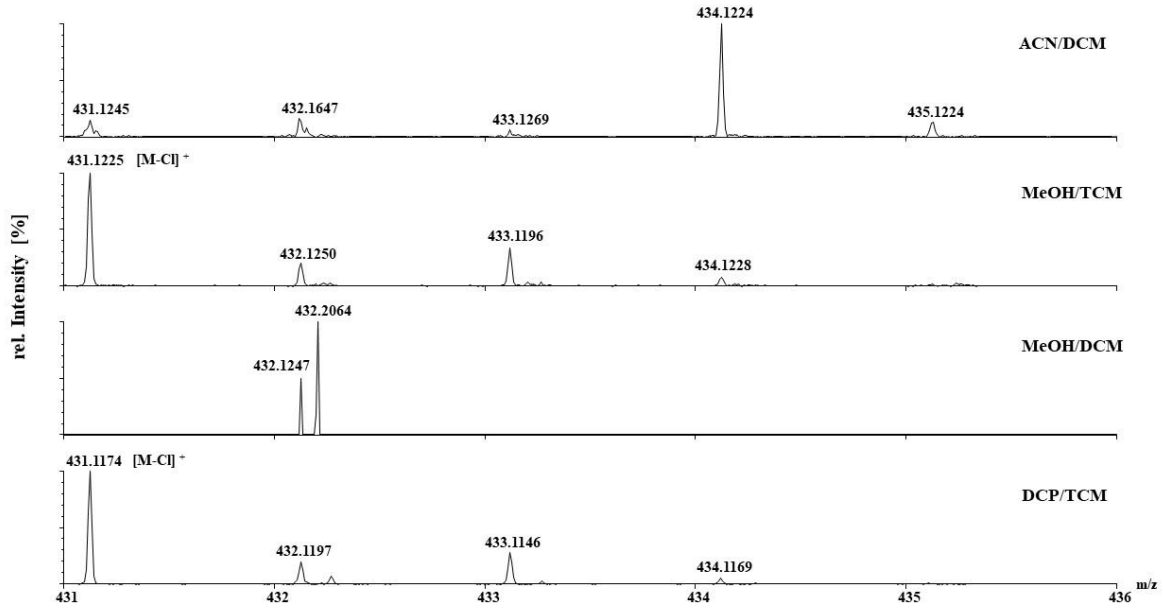

Figure 15: Comparison of the different solvent mixtures of compound **No.6**; Instrument: Synapt^{TM} G2 HDMS

In general, it can be said that the choice of solvent mixtures for the analysis of coordination compounds is often decisive for the result of a measurement. It is important to find a solvent in which the complex is present in a stable form, so that it can be analyzed afterwards. This statement can be supported by the fact that coordination compounds are generally very sensitive substances which, in combination with many solvents, often tend to decompose. Table 9 below lists the best solvent mixtures for all complexes analyzed.

Table 9: Ideal solvent mixtures for all analyzed coordination compounds

Complex	**Solvent mixture 1:1 (v/v)**
1	DCP/TCM
2	ACN/DCM
3	MeOH/DCM
4	ACN/DCM
5	MeOH/DCM
6	DCP/TCM
7	MeOH/TCM
8	MeOH/DCM
9	MeOH/DCM
10	ACN/DCM
11	ACN/DCM
12	MeOH/DCM
13	MeOH/TCM
14	ACN/DCM
15	ACN/DCM
16	MeOH/TCM
17	MeOH/DCM
18	MeOH/TCM

4.1.3 Measurements with high-resolution accurate mass MALDI MS

The following measurements were all performed with a high-resolution MALDI MS, the Synapt^{TM} G2 HDMS. All 18 coordination compounds selected were investigated and their characteristic isotope patterns were compared with those of a calculated spectrum. In addition, the mass error was determined in order to establish whether the compound was indeed the one in question.

High resolution spectra are necessary to determine the accurate mass of a compound and to identify reliably. Due to software limitations, the accurate mass of this instrument cannot be determined directly from the continuous spectrum. For this reason all masses listed below were taken from the centroid mode and corrected with those in the following spectra.

4.1.3.1 Coordination compounds with vanadium as metal center

Figure 17- Figure 21 show sections of the spectra of all measured coordination compounds (**No.1**-**No.3**) with a vanadium metal center. The complexes **No. 1** and **No. 2** are compounds with, among others, three chlorides each as ligands. Looking at Figure 17 and Figure 19, the isotope pattern of the halide is clearly visible. Vanadium itself has no characteristic isotope pattern. It is particularly noticeable that both complexes are detected as $[M\text{-}Cl]^+$ in the spectrum. This indicates the loss of a halide during the ionization process. Through the input of the laser beam, which should cause ablation of the sample material and its subsequent ionization, a high amount of energy is transferred to the sample, which can lead to a part of it, in this case a halide, being removed.

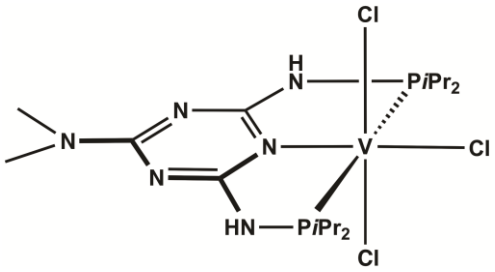

Figure 16: Chemical structure of $[V(Triaz^{NMe2}\text{-}i\text{Pr})Cl_3]$ (**No.1**)

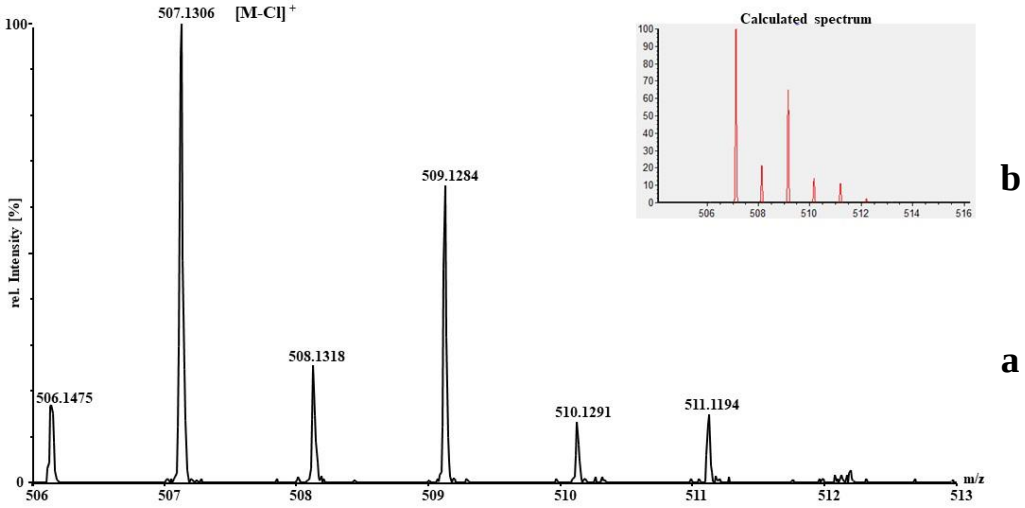

Figure 17: (a) Magnified view of the $[M\text{-}Cl]^+$ isotope pattern of the compound **No.1**; (b) calculated isotope pattern

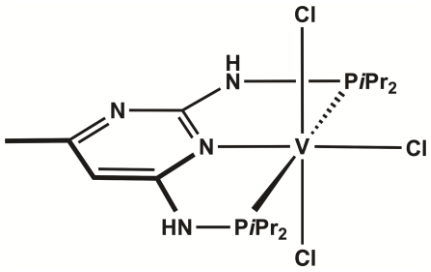

Figure 18: Chemical structure of $[V(Pym^{Me}\text{-}i\text{Pr})Cl_3]$ (**No.2**)

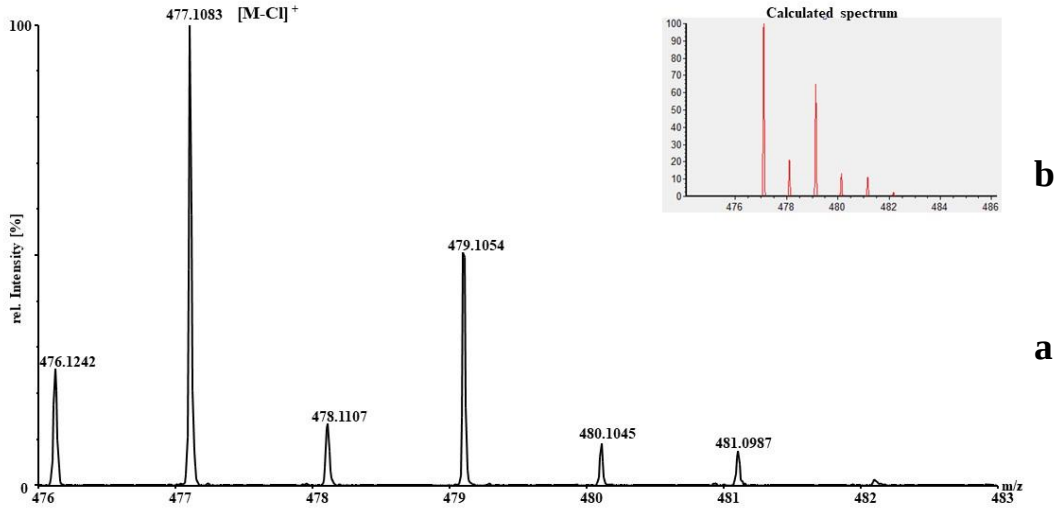

Figure 19: (a) Magnified view of the $[M\text{-}Cl]^+$ isotope pattern of the compound **No.2**; (b) calculated isotope pattern

Complex **No. 3**, whose spectrum is shown in Figure 21, is vanadyl acetylacetonate. In contrast to the previous compounds, it does not contain halides as ligands. The complex could be detected in the form of a sodium adduct. Therefore, ligand removal does not take place here either.

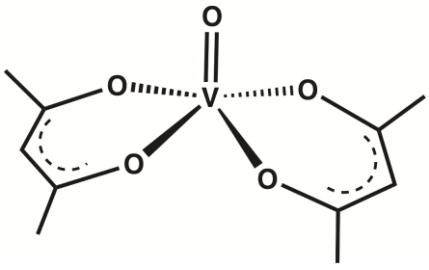

Figure 20: Chemical structure of $[V(acac)_2(O)]$ (**No.3**)

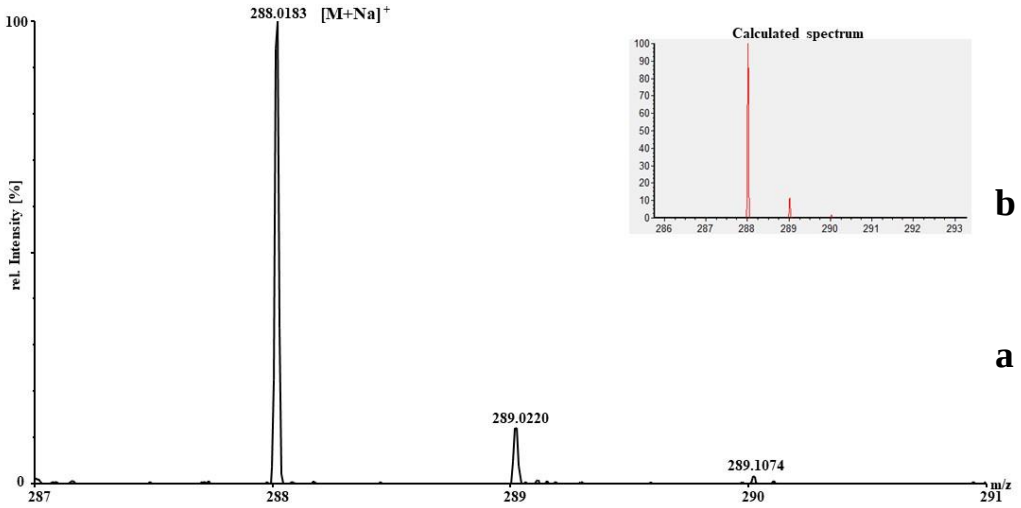

Figure 21: (a) Magnified view of the $[M+Na]^+$ isotope pattern of the compound **No.3**; (b) calculated isotope pattern

The mass error Δm indicates to what extent the measured value of the monoisotopic mass of a molecule deviates from its theoretical value. Most journals require a mass accuracy of less than 5 ppm to ensure that the analyzed sample is indeed the molecule in question. The values for the mass error of the coordination compounds with vanadium as metal center can be found in Table 10.

Table 10: Mass error of the analyzed vanadium compounds

Complex	**Δm [ppm]**
1	3.6
2	2.8
3	3.5

4.1.3.2 Coordination compounds with chromium as metal center

In this chapter the isotope patterns of the investigated chromium compounds are presented (Figure 23 & Figure 25). Amongst others, complex **No.4** has three carbon monoxide molecules as ligands. These can separated from the molecule both neutrally and as charge carriers during ionization. Furthermore, the complex tend to absorb light at different wavelengths, which obviously includes the wavelength of the Nd:YAG lasers used (λ=355 nm). This leads to the loss of the CO molecules. In this case, this also explains why the molecule could be detected as $[M\text{-}3CO+Cl]^+$.

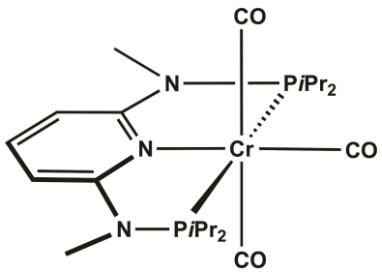

Figure 22: Chemical structure of $[Cr(PNP^{NMe}\text{-}i\text{Pr})(CO)_3]$ (**No.4**)

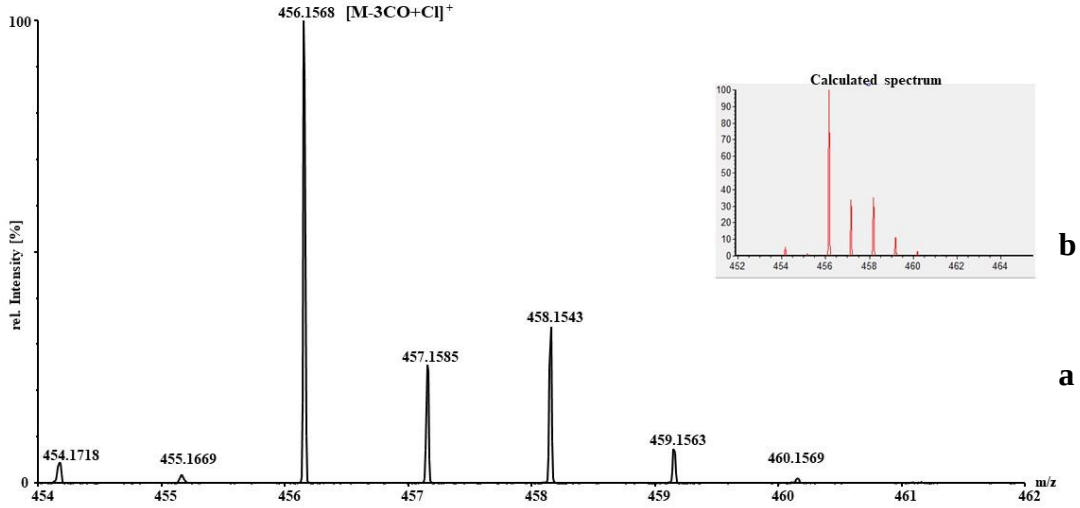

Figure 23: (a) Magnified view of the $[M-3CO+Cl]^+$ isotope pattern of the compound **No.4**; (b) calculated isotope pattern

Compound **No.5** is chromium acetylacetonate. It can be detected in the spectrum as a sodium adduct. Here, a relationship can already be observed in the measurement result of complex **No.3** and complex **No.5**. Both coordination compounds have the same ligand system and could be detected as sodium adducts.

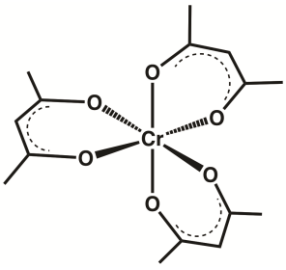

Figure 24: Chemical structure of $[Cr(acac)_3]$ (**No.5**)

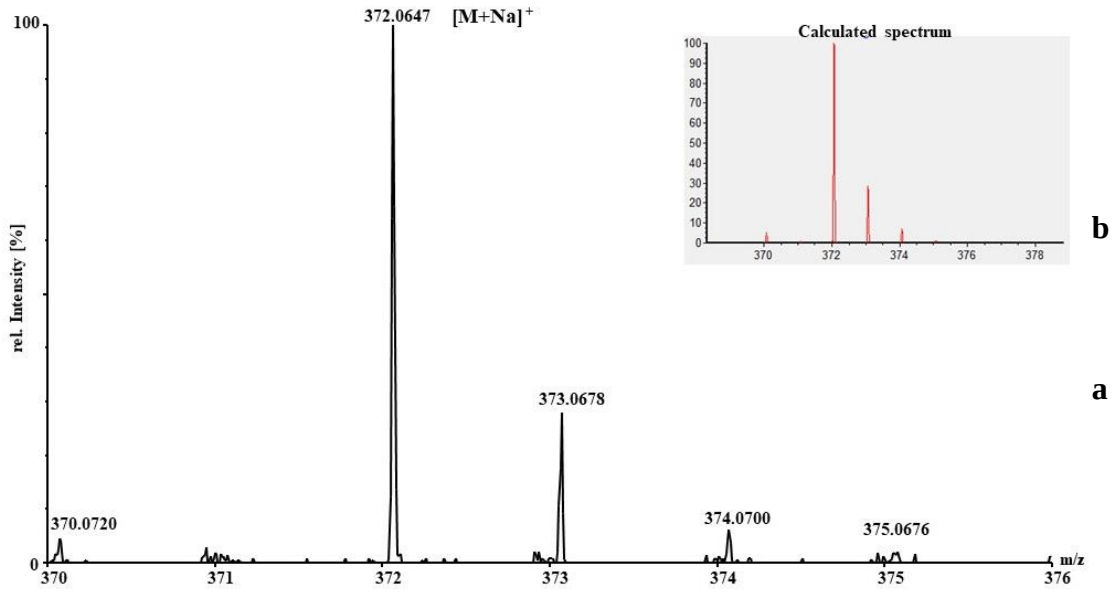

Figure 25: (a) Magnified view of the $[M+Na]^+$ isotope pattern of the compound **No.5**; (b) calculated isotope pattern

The mass error of the analyzed chromium compounds is listed in Table 11.

Table 11: Mass error of the analyzed chromium compounds

Complex	**Δm [ppm]**
4	3.8
5	3.1

4.1.3.3 Coordination compounds with manganese as metal center

This chapter deals with the results of the analysis of manganese complexes. The complexes **No. 6** and **7** (spectra are shown in Figure 27 & Figure 29) again have halides

(chlorine and bromine) as ligands. In the course of ionization, these are removed from the compound, resulting in the complexes being visible in the spectrum in the form of $[M\text{-}Cl]^+$ and $[M\text{-}Br]^+$.

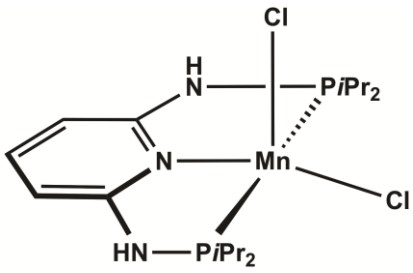

Figure 26: Chemical structure of $[Mn(PNP^{NH}\text{-}i\text{Pr})Cl_2]$ (**No.6**)

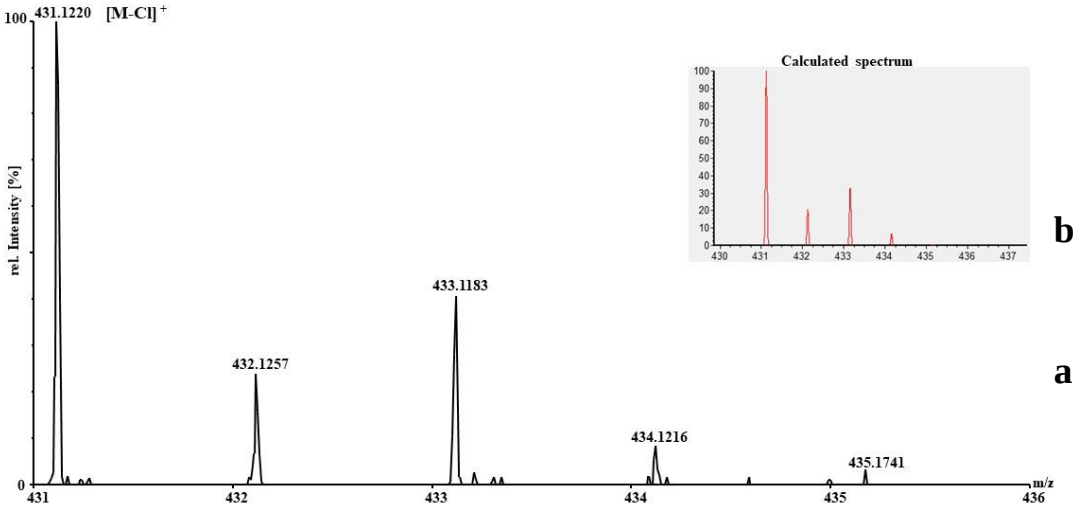

Figure 27: (a) Magnified view of the $[M\text{-}Cl]^+$ isotope pattern of the compound **No.6**; (b) calculated isotope pattern

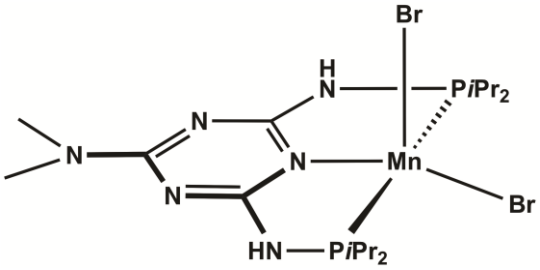

Figure 28: Chemical structure of $[Mn(Triaz^{NMe2}\text{-}i\text{Pr})Br_2]$ **(No.7)**

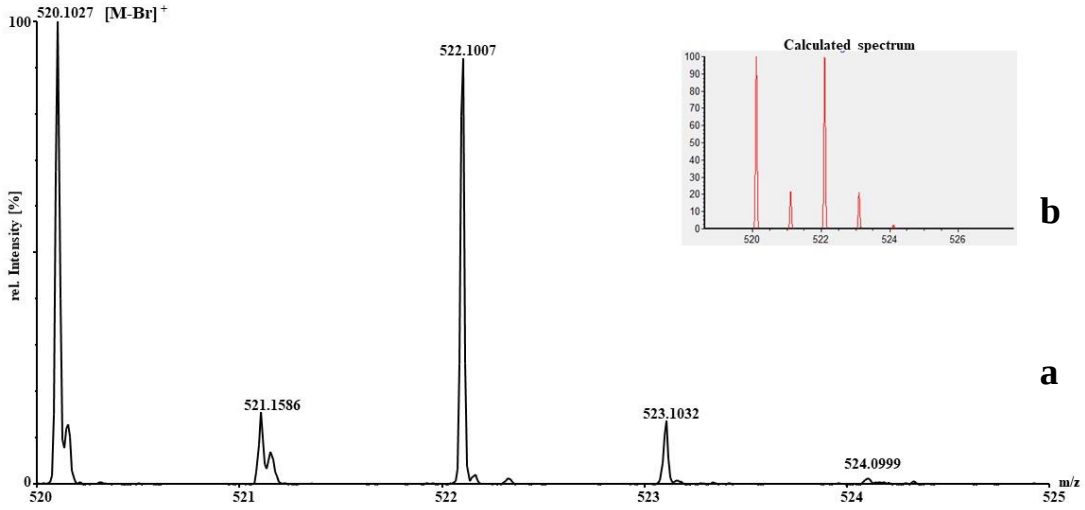

Figure 29: (a) Magnified view of the $[M\text{-}Br]^+$ isotope pattern of the compound **No.7**; (b) calculated isotope pattern

Compound **No.8** (Figure 31) could be detected as sodium adduct in the spectrum. Like vanadium, the manganese atom itself has no characteristic isotope pattern, as can be seen from the spectrum.

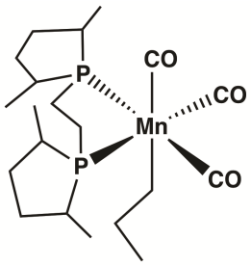

Figure 30: Chemical structure of $[Mn(me\text{-}bpe)(CO)_3(C_3H_7)]$ (**No.8**)

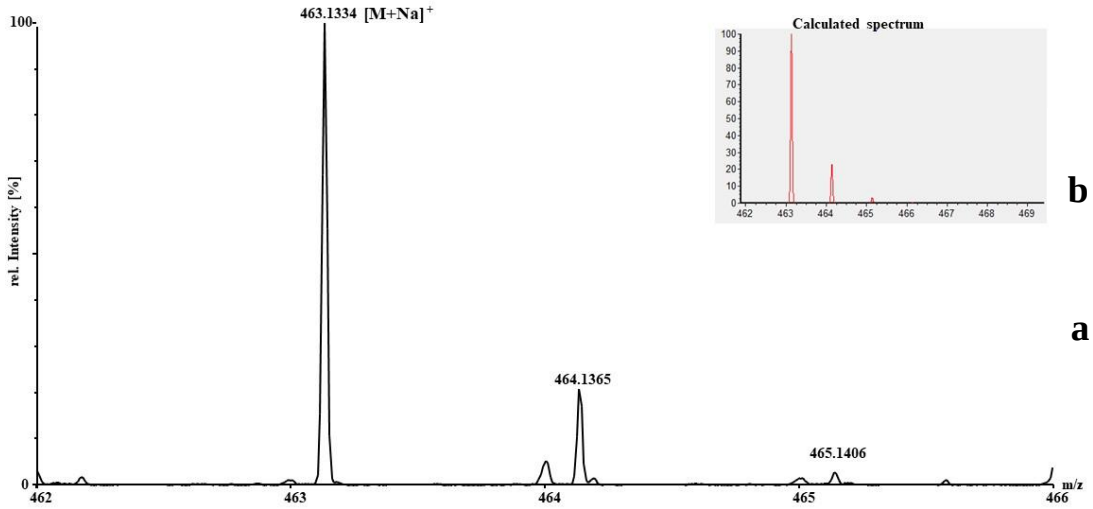

Figure 31: (a) Magnified view of the $[M+Na]^+$ isotope pattern of the compound **No 8**; (b) calculated isotope pattern

Inter alia, coordination compound **No.9** has three carbon monoxide ligands in addition to one bromine atom. If a look at the spectrum is taken, it is apparent that all three CO atoms are cleaved off during ionization. The bromine atom is still present, which is reflected in the isotope pattern. In the course of this work it becomes clear that CO ligands preferentially cleave off in the ionization process.

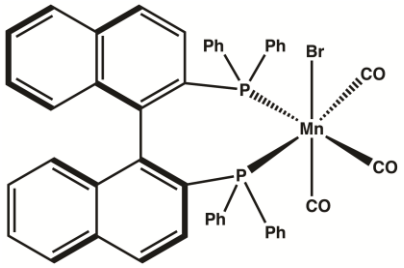

Figure 32: Chemical structure of $[Mn(BINAP)(CO)_3Br]$ (**No.9**)

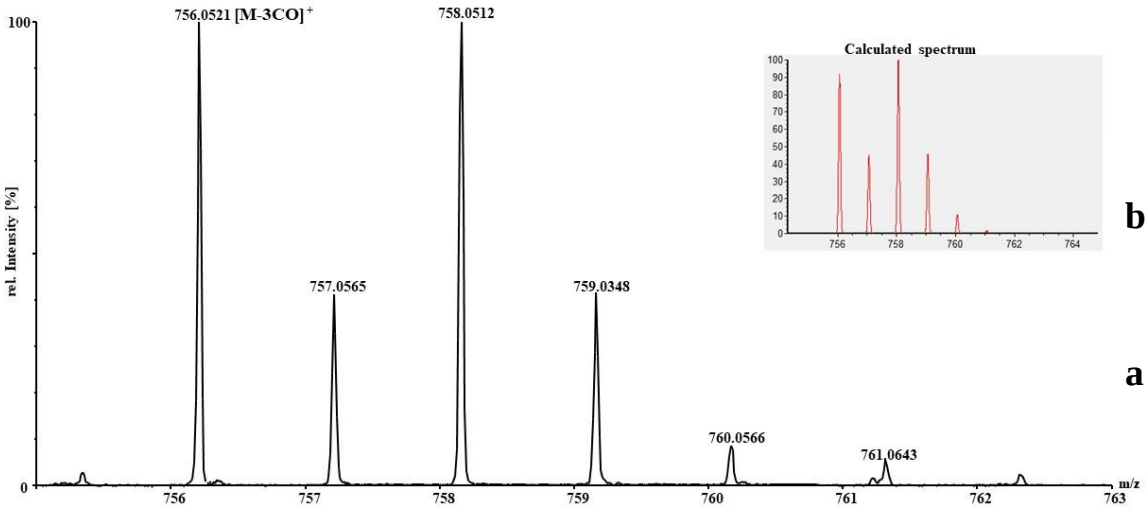

Figure 33: (a) Magnified view of the $[M-3CO]^+$ isotope pattern of the compound **No.9**; (b) calculated isotope pattern

The mass error of the analyzed manganese compounds is listed in Table 12.

Table 12: Mass error of the analyzed manganese compounds

Complex	**Δm [ppm]**
6	1.6
7	1.5
8	0.02
9	2.2

4.1.3.4 Coordination compounds with iron as metal center

In the following subchapter all iron complexes analyzed are discussed. In the case of complexes **No.10** & **11** these are compounds, which have two bromine atoms as ligands.

One of these bromine atoms is cleaved off during ionization. When looking at the spectra in Figures 35 & 37, it is conspicuous that the compounds are detected in the form of $[M\text{-}Br+2O]^+$ in the spectrum. This is due to the fact that, as mentioned in previous chapters, the compounds are not very stable and because of the extreme conditions prevailing in the instrument itself (vacuum, high energy input by the laser). This can cause molecules to be detected in a form that would not be present at room temperature and atmospheric pressure. It is likely that the molecule is present in its oxidized form. Assuming that oxygen attaches to the two phosphorus atoms of the PNP ligand system of the substance.

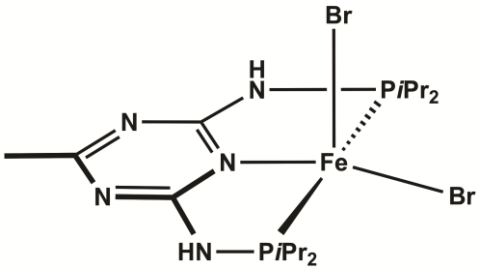

Figure 34: Chemical structure of $[Fe(Triaz^{Me}\text{-}i\text{Pr})Br_2]$ (**No.10**)

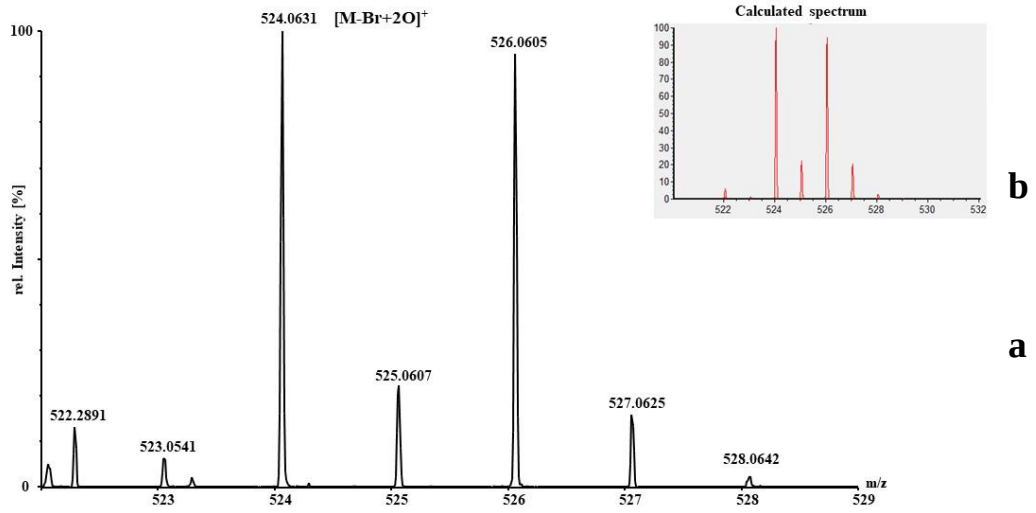

Figure 35: (a) Magnified view of the $[M\text{-}Br+2O]^+$ isotope pattern of the compound **No.10**; (b) calculated isotope pattern

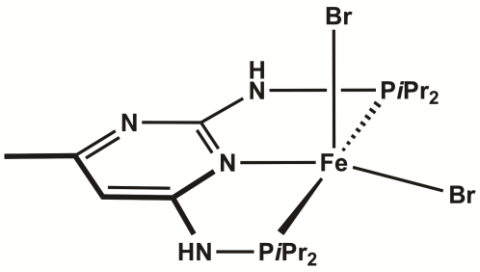

Figure 36: Chemical structure of [Fe(Pym^{Me}-*i*Pr)Br$_2$] (**No.11**)

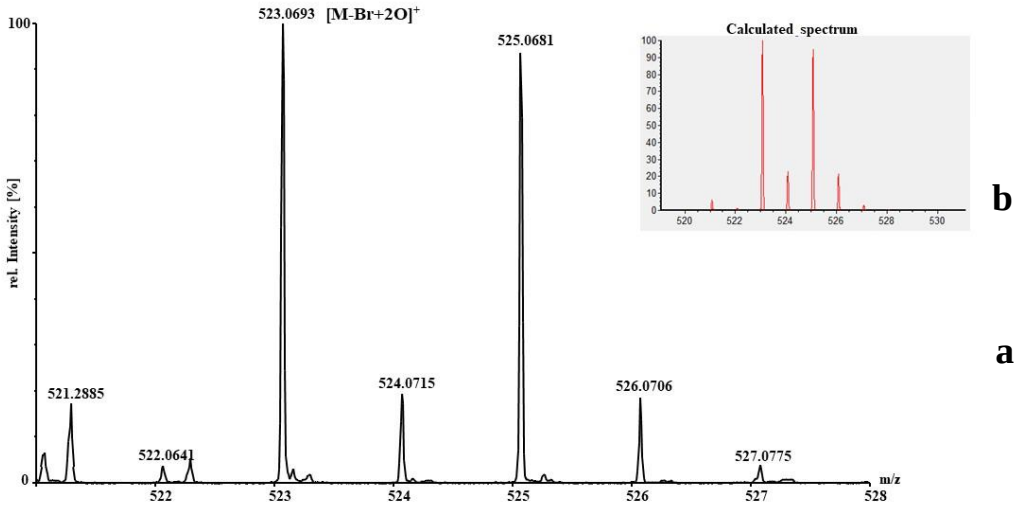

Figure 37: (a) Magnified view of the [M-Br+2O]$^+$ isotope pattern of the compound **No.11**; (b) calculated isotope pattern

Compound **No.12** is iron acetylacetonate. As with the other complexes, where acetylacetonates acted as ligands, it can also be detected as [M+Na]$^+$.

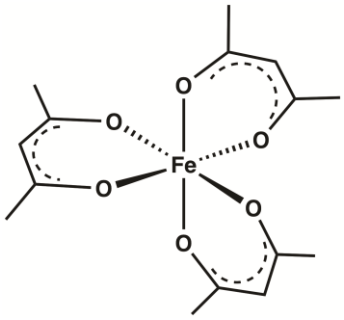

Figure 38: Chemical structure of $[Fe(acac)_3]$ (**No.12**)

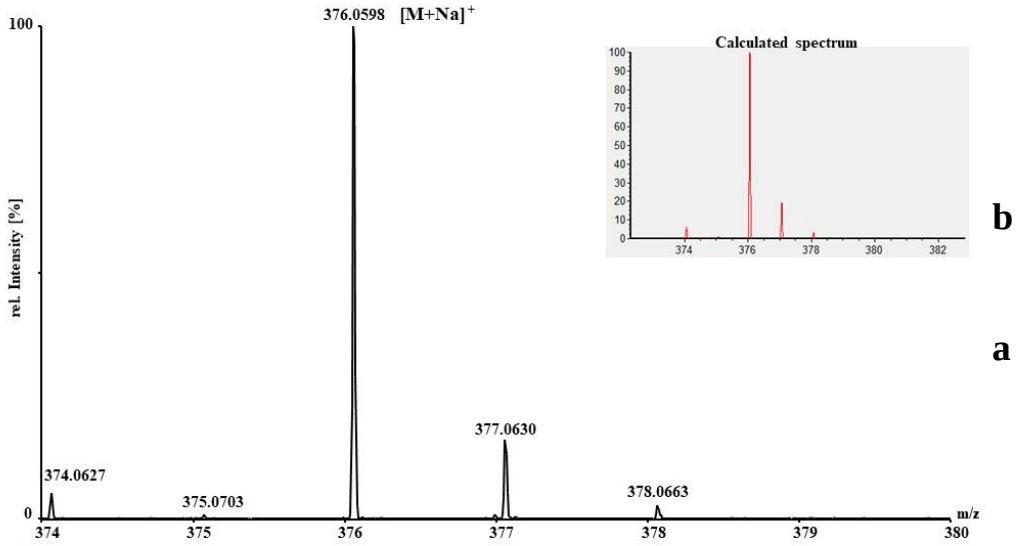

Figure 39: (a) Magnified view of the $[M+Na]^+$ isotope pattern of the compound **No. 12**; (b) calculated isotope pattern

Figure 41 provides the isotope pattern of the $[M\text{-}CO\text{-}Cl]^+$ molecular ion peak of complex **No.13**. In addition to the neutral removal of the CO molecule, a removal of a chlorine radical takes place.

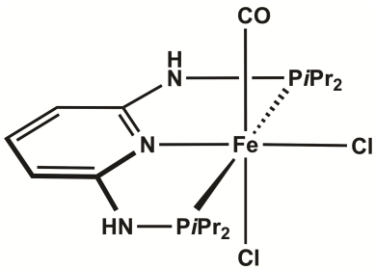

Figure 40: Chemical structure of [Fe(PNP^{NH}-*i*Pr)(CO)Cl$_2$] (**No.13**)

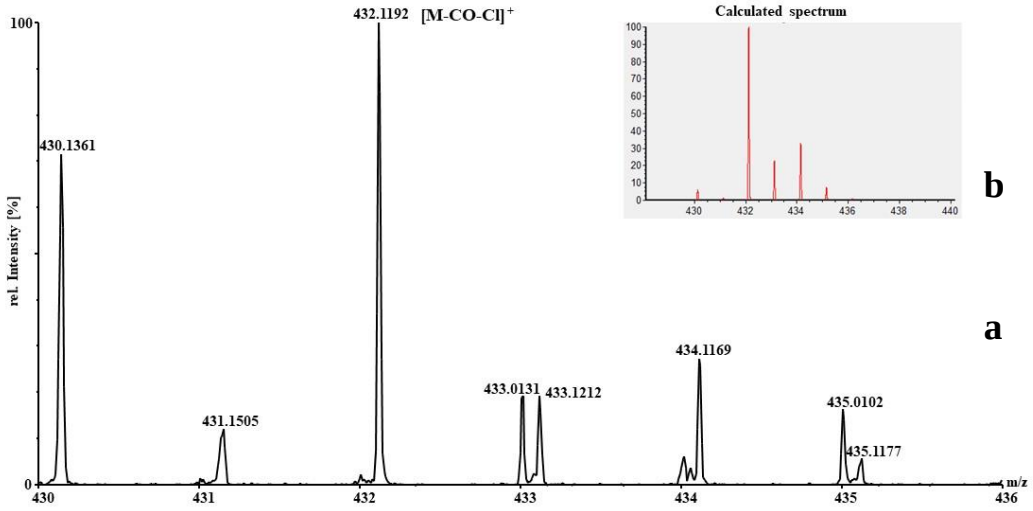

Figure 41: (a) Magnified view of the [M-CO-Cl]$^+$ isotope pattern of the compound **No.13**; (b) calculated isotope pattern

The complexes **No.14** and **15**, whose spectra are shown in Figure 43 and Figure 45, can be detected as [M]$^+$ molecular ion. The chlorine atoms present in compound **No.14** are also reflected in the isotope pattern. The isotope patterns of the real measurement correspond in both cases with the calculated isotope patterns.

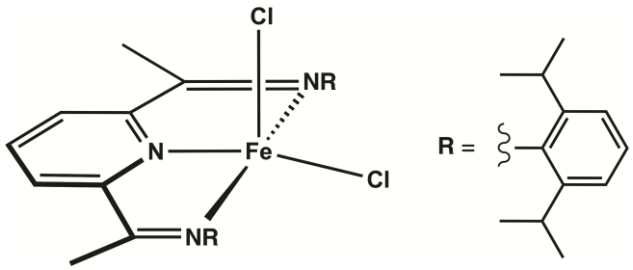

Figure 42: Chemical structure of [Fe(NNN-PDI)Cl_2] (**No.14**)

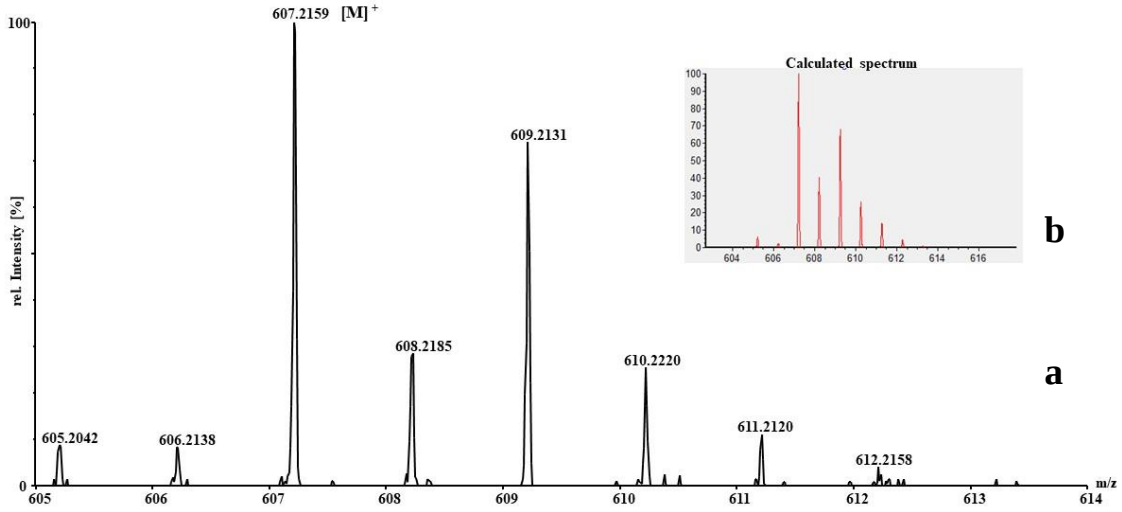

Figure 43: (a) Magnified view of the $[M]^+$ isotope pattern of the compound **No. 14**; (b) calculated isotope pattern

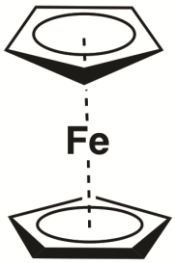

Figure 44: Chemical structure of Cp_2Fe (**No.15**)

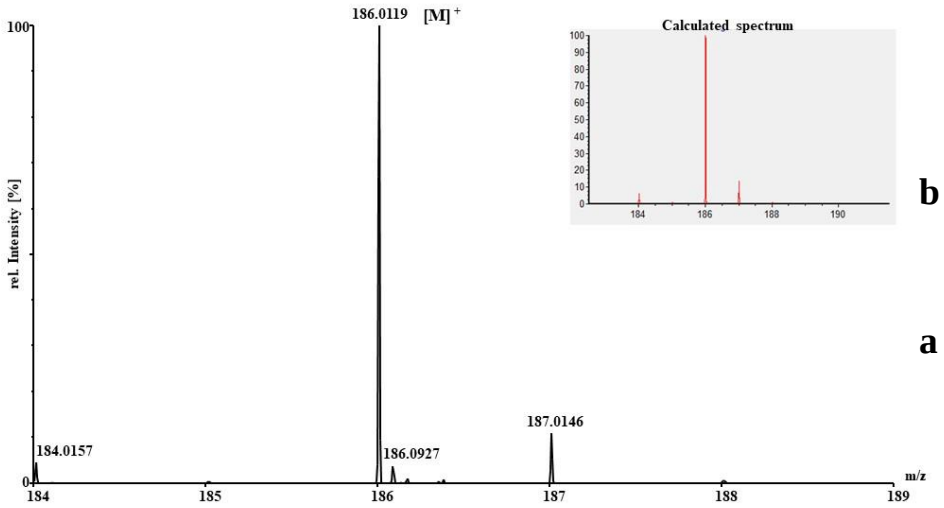

Figure 45: (a) Magnified view of the $[M]^+$ isotope pattern of the compound **No.15**; (b) calculated isotope pattern

The mass error of the analyzed iron compounds is listed in Table 13.

Table 13: Mass error of the analyzed iron compounds

Complex	**Δm [ppm]**
10	1.5
11	1.7
12	4.8
13	2.3
14	3.1
15	4.0

4.1.3.5 Coordination compounds with cobalt as metal center

The examined cobalt complexes **No.16** and **No.17** (spectra see Figure 47 & Figure 49) can both be detected as $[M\text{-}Cl]^+$ peak in the spectrum. As in the case of manganese and vanadium, also cobalt has no specific isotope pattern. The presence of the chlorine atoms, which act as ligands, can be seen in the isotope pattern of the spectrum.

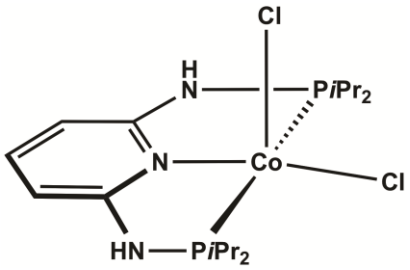

Figure 46: Chemical structure of $[Co(PNP^{NH}\text{-}i\text{Pr})Cl_2]$ (**No.16**)

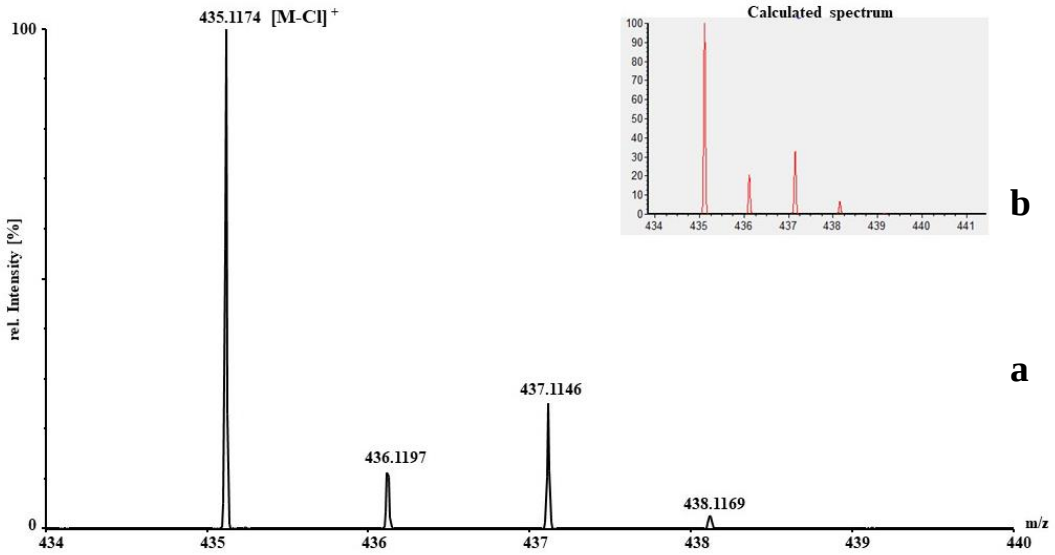

Figure 47: (a) Magnified view of the $[M\text{-}Cl]^+$ isotope pattern of the compound **No. 16**; (b) calculated isotope pattern

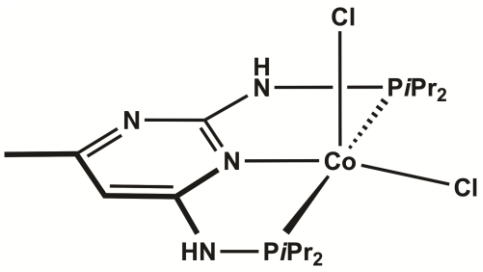

Figure 48: Chemical structure of [Co(Pym^{Me}-*i*Pr)Cl_2] (**No.17**)

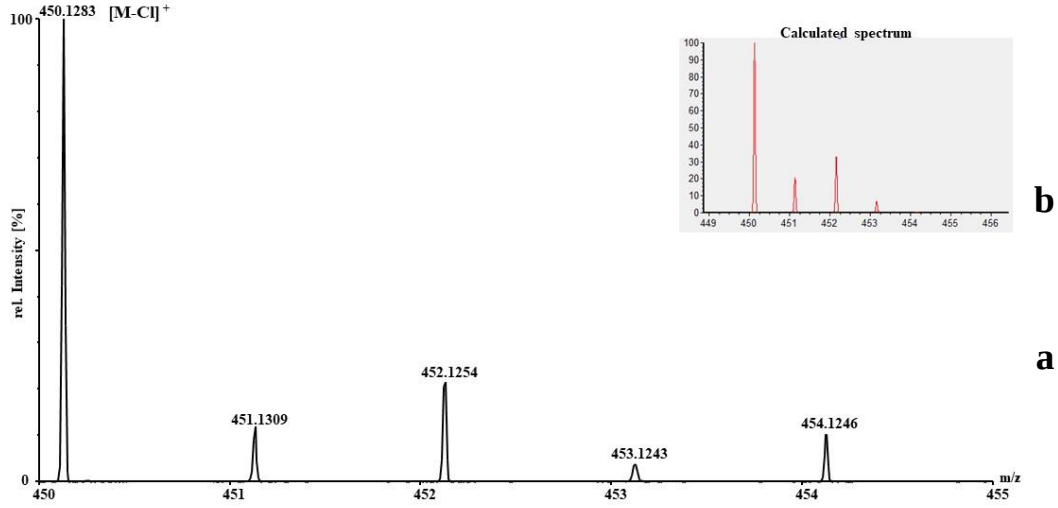

Figure 49: (a) Magnified view of the [M-Cl]$^+$ isotope pattern of the compound **No.17**; (b) calculated isotope pattern

The mass error of the analyzed cobalt compounds is listed in Table 14.

Table 14: Mass error of the analyzed cobalt compounds

Complex	**Δm [ppm]**
16	2.4
17	2.0

4.1.3.6 Coordination compounds with nickel as metal center

In this chapter a coordination compound with nickel as metal center is presented. The magnified view of the spectrum and its calculated isotope pattern is shown in Figure 51. Amongst others, this complex has two chlorine atoms as ligands. The compound could be detected as $[M\text{-}Cl]^+$, i.e. with the loss of one chlorine atom. As already mentioned several times in the previous chapters, this is due to a cleavage during ionization.

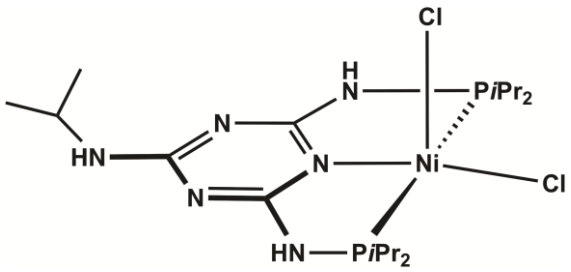

Figure 50: Chemical structure of [Ni(Triaz^{NiPr}-*i*Pr)Cl_2] (**No.18**)

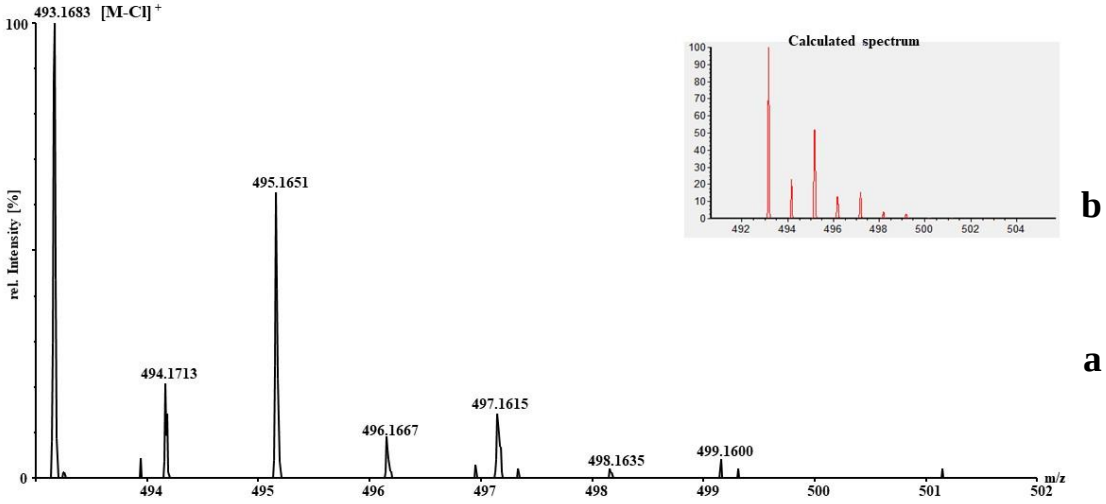

Figure 51: (a) Magnified view of the $[M\text{-}Cl]^+$ isotope pattern of the compound **No. 18**; (b) calculated isotope pattern

The mass error of the analyzed nickel compound is listed in Table 15.

Table 15: Mass error of the analyzed nickel compound

Complex	**Δm [ppm]**
18	2.7

4.1.4 Comparison of different ionization techniques

In this chapter, the differences of various instruments and ionization techniques are discussed using some of the previous complexes as examples. In selecting the data presented, the focus was placed on being able to show a representative selection of the overall measurements. Figure 52 compares spectra of compound **No.16** measured with Agilent 6545 QTOF (ESI), ultrafleXtreme™ (MALDI) and Synapt™ G2 HDMS (MALDI). On closer examination of the figure, it becomes clear that the complex with all instruments is present as a $[M\text{-}Cl]^+$ peak in the spectrum. In the spectrum of the ultrafleXtreme™, the $[M]^+$ peak could also be detected, but at a much lower intensity. This may be due to the fact that the mass spectrometer is a RTOF, whereas the other instruments have a coupling of quadrupole and RTOF. This makes it possible that the $[M]^+$ ions decompose during linear flight path and no longer reach the detector.

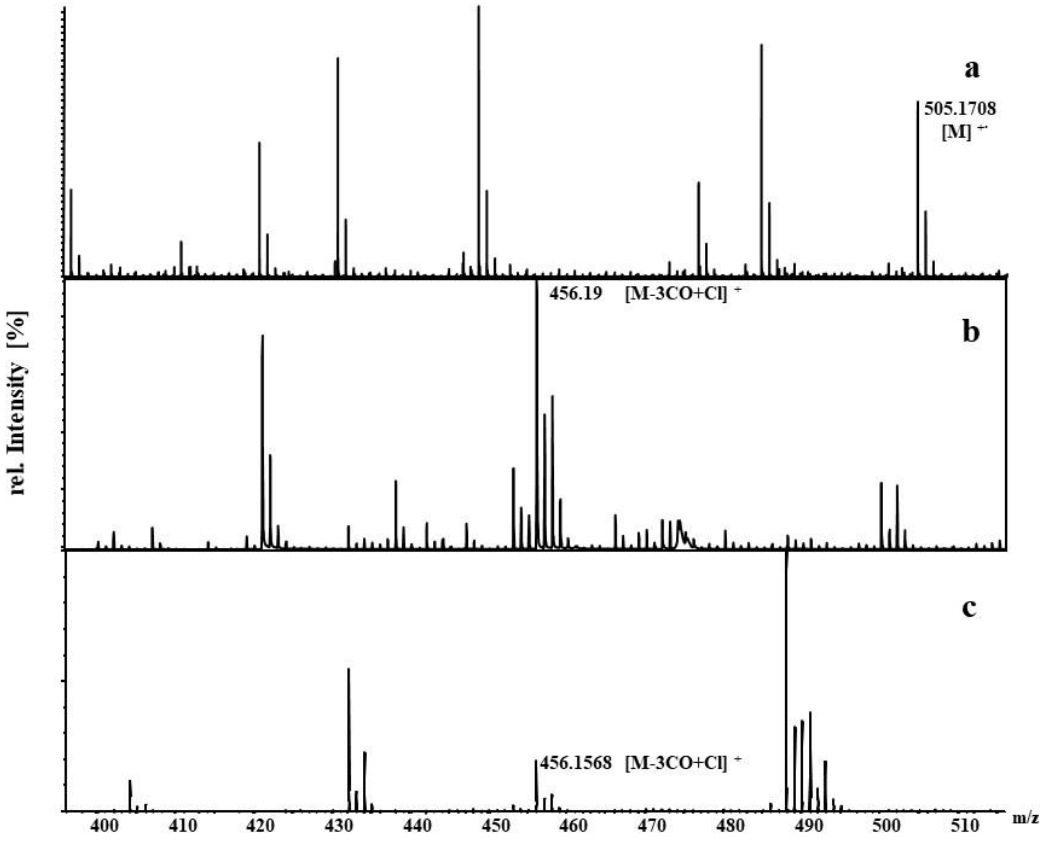

Figure 52: Comparison of different ionization techniques of complex **No.16** utilizing **(a)** Agilent 6545 QTOF (ESI), **(b)** ultrafleXtreme™ (MALDI) and Synapt™ G2 HDMS (MALDI) **(c)**

In the case of complex **No.18** (see Figure 53), the $[M\text{-}Cl]^+$ peak is also visible with all ionization techniques.

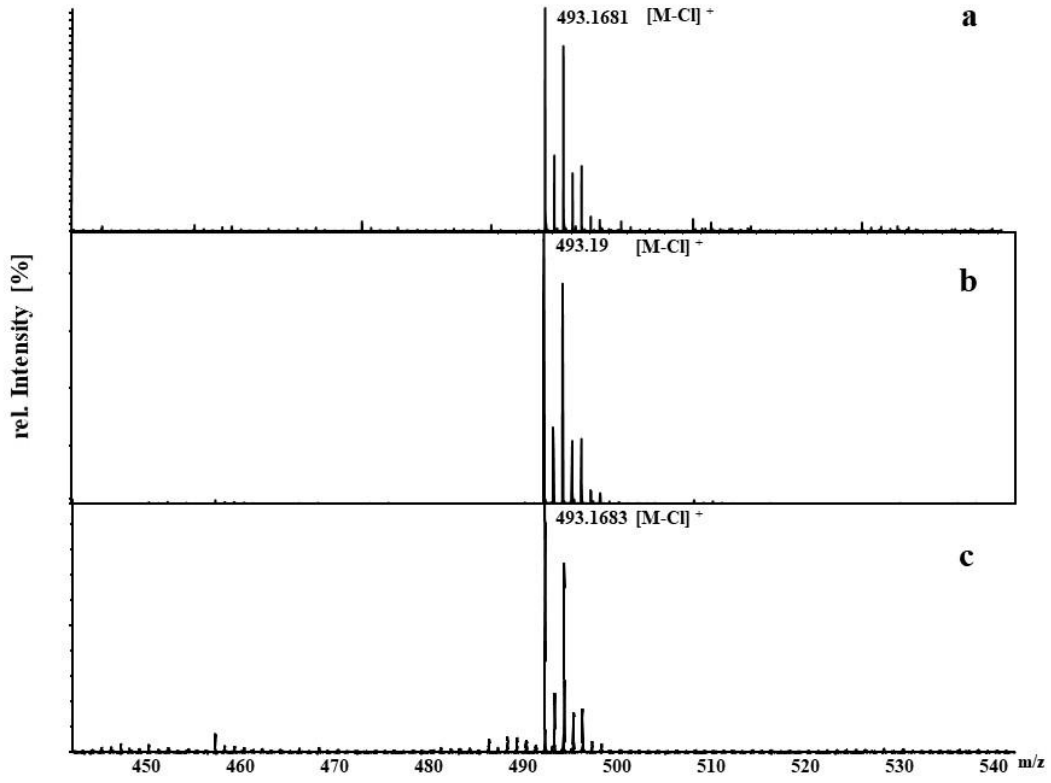

Figure 53: Comparison of different ionization techniques of complex **No.18** utilizing **(a)** Agilent 6545 QTOF (ESI), **(b)** ultrafleXtreme^{TM} (MALDI) and Synapt^{TM} G2 HDMS (MALDI) **(c)**

The spectra of complex **No.4** (Figure 54) show clear differences between the ionization techniques MALDI and ESI. While ESI MS detects the $[M]^+$ peak of the coordination compound, MALDI MS results in the loss of carbon monoxide molecules during ionization. In addition, a binding of the chloride ion takes place. As a reminder, a sodium salt (NaCl or NaBr) was added to all compounds. In the course of this, the detected metastable states may occur due to the conditions in the device itself.

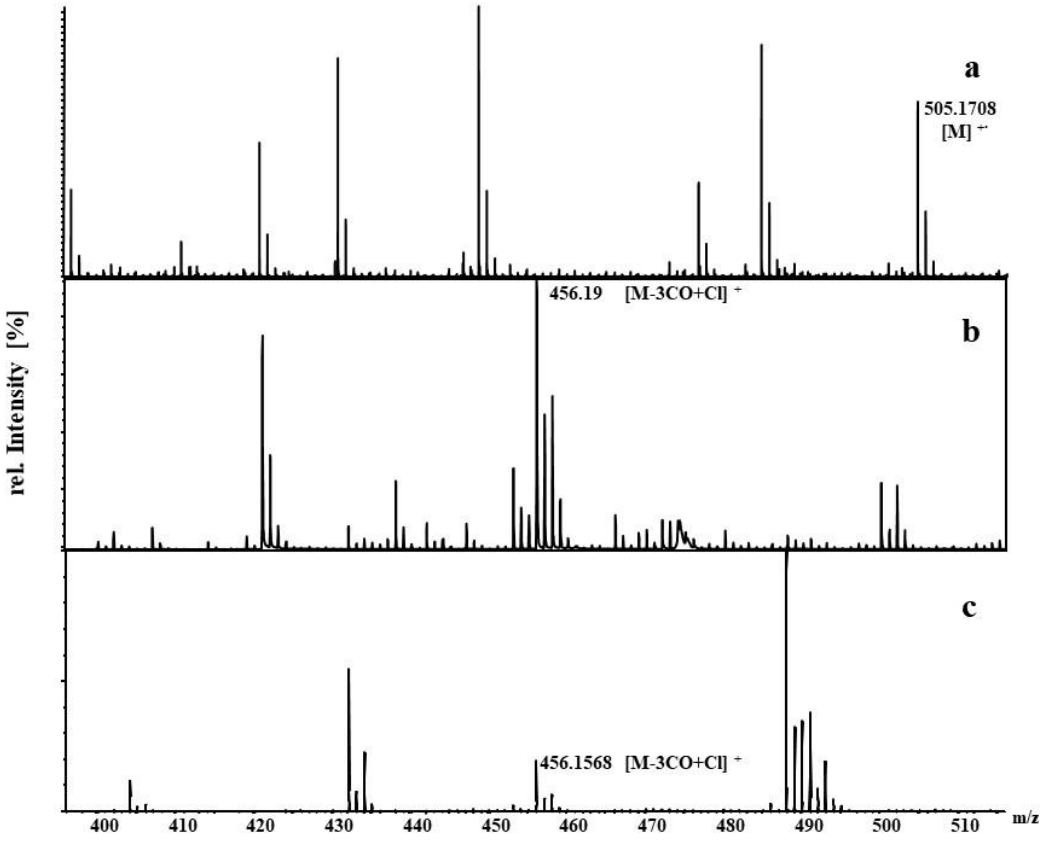

Figure 54: Comparison of different ionization techniques of complex **No.4** utilizing **(a)** Agilent 6545 QTOF (ESI), **(b)** ultrafleXtreme^{TM} (MALDI) and Synapt^{TM} G2 HDMS (MALDI) **(c)**

Considering the spectra of complex **No.10 (**Figure 55**)**, it becomes clear that the compound is not detectable by ESI MS. With MALDI MS it is possible that the coordination compound can be detected as $[M\text{-}Br+2O]^+$. This molecular ion is again a metastable state, which is owed to the conditions in the device. This also reveals one of the essential differences in ionization between ESI and MALDI. With MALDI the sample is introduced into the instrument in solid state, with ESI in liquid state. The fact that the sample is in a liquid phase state when it is introduced into the instrument prohibits the formation of molecular ions as is possible with MALDI.

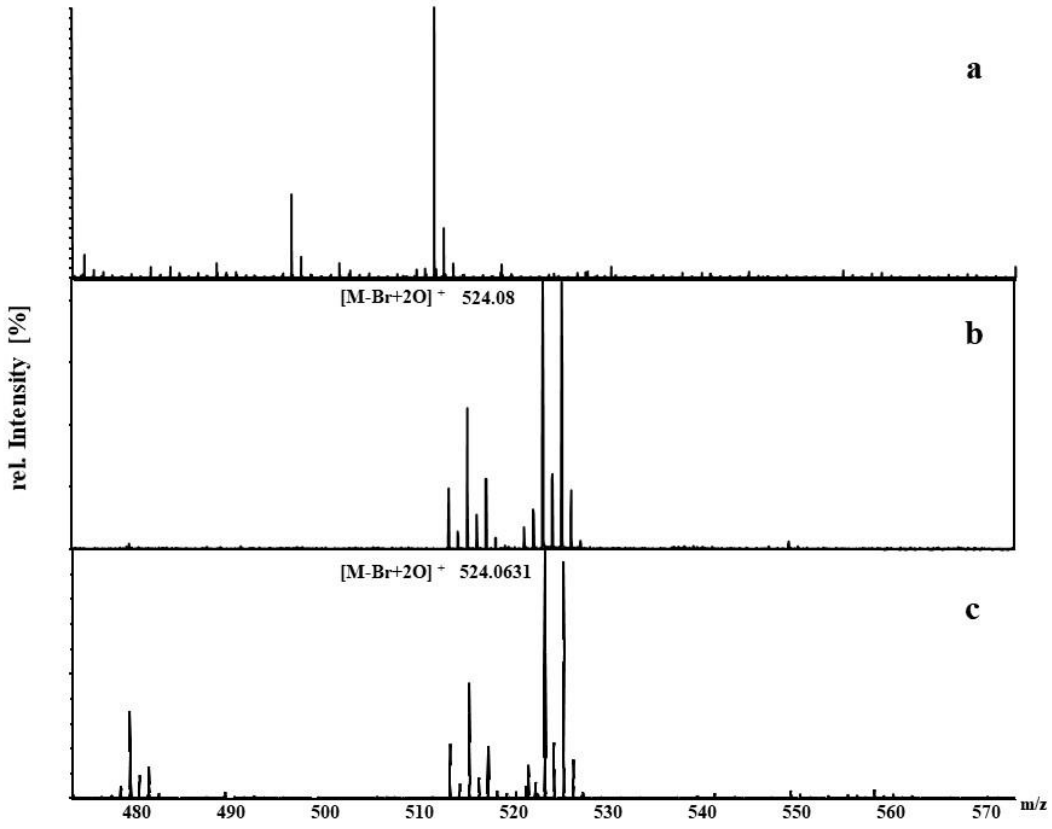

Figure 55: Comparison of different ionization techniques of complex **No.10** utilizing **(a)** Agilent 6545 QTOF (ESI), **(b)** ultrafleXtreme™ (MALDI) and Synapt™ G2 HDMS (MALDI) **(c)**

In summary, it can be said that there are definitely differences of the molecule as ion in the mass spectrum, depending on the selected ionization technique. As already mentioned, the spectra discussed above serve to provide a representative section of the overall measurements. Therefore the results of all measurements are given in Table 16.

Table 16: Summary of the comparison of all measured coordination compounds with different ionization techniques

	Chemical formula	**Monoisotopic mass**	**Synapt™ G2 HDMS**	**ultrafleXtreme™**	**Agilent 6545 QTOF**
1	$C_{17}H_{36}Cl_3N_6P_2V$	542.0976	$[M\text{-}Cl]^+$	$[M\text{-}Cl]^+$	(-)
2	$C_{17}H_{34}Cl_3N_4P_2V$	512.0758	$[M\text{-}Cl]^+$	$[M\text{-}Cl]^+$	(-)
3	$C_{10}H_{14}O_5V$	265.0275	$[M+Na]^+$	$[M+Na]^+$	$[M+Na]^+$
4	$C_{22}H_{37}CrN_3O_3P_2$	505.1709	$[M\text{-}3CO+Cl]^+$	$[M\text{-}3CO+Cl]^+$	$[M]^{+\cdot}$
5	$C_{15}H_{21}CrO_6$	349.0737	$[M+Na]^+$	$[M+Na]^+$	$[M+Na]^+$
6	$C_{17}H_{33}Cl_2MnN_3P_2$	466.0901	$[M\text{-}Cl]^+$	$[M\text{-}Cl]^+$	(-)
7	$C_{17}H_{36}Br_2MnN_6P_2$	599.0218	$[M\text{-}Br]^+$	$[M\text{-}Br]^+$	(-)
8	$C_{20}H_{35}MnO_3P_2$	440.1436	$[M+Na]^+$	$[M+Na]^+$	$[M+Na]^+$
9	$C_{47}H_{32}BrMnO_3P_2$	840.0385	$[M\text{-}3CO]^+$	$[M\text{-}3CO]^+$	(-)
10	$C_{16}H_{33}Br_2FeN_5P_2$	570.9921	$[M\text{-}Br+2O]^+$	$[M\text{-}Br+2O]^+$	(-)
11	$C_{17}H_{34}Br_2FeN_4P_2$	569.9969	$[M\text{-}Br+2O]^+$	$[M\text{-}Br+2O]^+$	(-)
12	$C_{15}H_{21}FeO_6$	353.0682	$[M+Na]^+$	$[M+Na]^+$	$[M+Na]^+$
13	$C_{18}H_{33}Cl_2FeN_3OP_2$	495.0819	$[M\text{-}CO\text{-}Cl]^+$	$[M\text{-}CO\text{-}Cl]^+$	(-)
14	$C_{33}H_{43}Cl_2FeN_3$	607.2177	$[M]^+$	$[M]^+$	$[M\text{-}Cl]^+$
15	$C_{10}H_{10}Fe$	186.0126	$[M]^+$	$[M]^+$	$[M]^+$
16	$C_{17}H_{33}Cl_2CoN_3P_2$	470.0853	$[M\text{-}Cl]^+$	$[M\text{-}Cl]^+$	$[M\text{-}Cl]^+$
17	$C_{17}H_{34}Cl_2CoN_4P_2$	485.0962	$[M\text{-}Cl]^+$	$[M\text{-}Cl]^+$	$[M\text{-}Cl]^+$
18	$C_{18}H_{38}Cl_2N_6NiP_2$	528.1358	$[M\text{-}Cl]^+$	$[M\text{-}Cl]^+$	$[M\text{-}Cl]^+$

5 Conclusion

This thesis demonstrates the different facts of sample preparation and analysis of coordination compounds. Two different matrices were compared, which ultimately resulted in the conclusion that both lead to completely identical results (see section 4.1.1). In addition, all compounds were examined with four different solvent combinations (chapter 4.1.2). Most complexes could only be detected with one of these solvent mixtures which once again underlined the necessity of choosing the right solvent. Since coordination compounds often have special isotope patterns due to their metal center, but also because of some ligand systems (e.g. halides), these can be used as an indication that the target compound is actually the compound in question. For this reason, all investigated complexes were compared with the calculated isotope patterns. All compounds mentioned in the course of this study could thus be assigned to the respective molecule, not only on the basis of their accurate mass, but also with their isotope pattern.

Even though MALDI MS has not prevailed over the conventional analysis technique with ESI MS due to various factors (analysis of highly oxidation-sensitive complexes turns out to be difficult), this work can prove that it does indeed enjoy non-negligible advantages over ESI MS. For example, by optimizing the measurement parameters, it was possible to analyze all coordination compounds with one and the same measurement method. This allowed a batch measurement that did not require the presence of operators. In contrast, the parameters of the ESI MS measurements had to be individually adapted and optimized for each sample. Furthermore, this class of analytes tends to decompose in the dissolved state. This circumstance requires the samples to be measured immediately after adding the solvent. It should also be mentioned that ESI MS does not offer the possibility of lateral resolution and therefore no imaging experiments can be performed with this technique.

To sum up, MALDI MS is an underestimated but powerful technique for the analysis of coordination compounds which, despite its infrequent use, may offer an alternative and complement to ESI MS.

6 List of figures

7 List of tables

8 Abbreviations

ACN	Acetonitrile
APCI	Atmospheric-pressure chemical ionization
BuLi	Butyllithium
CDEM	Continuous dynode electron multiplier
CO	Carbon monoxide
DCM	Dichloromethane
DCP	Dichloropropane
DCTB	Trans-2-[3-(4-tert-Butylphenyl)-2-methyl-2-propenylidene]malononitrile
DHB	2,5-dihydroxy benzoic acid
DT	Dithranol
E_{el}	Electric potential energy
EI	Electron impact
E_k	Kinetic energy
EM	Electron multiplier
EPR	Electron paramagnetic resonance spectroscopy
ESI	Electrospray ionization
FT-ICR	Fourier-transform ion cyclotron resonance
HPLC	High-performance liquid chromatography

HR	High resolution
Hz	Hertz
IMS	Imaging mass spectrometry
IR	Infrared spectroscopy
ITO	Indium tin oxide coated glass slide
LTOF	Linear time-of-flight
m/z	Mass to charge ratio
MALDI	Matrix assisted laser desorption/ionization
MCP	Microchannel plate
MCTS	Multicellular tumor spheroids
MeOH	Methanol
MMI	Multimode ionization
MS	Mass spectrometry
NaBr	Sodium bromide
NaCl	Sodium chloride
Nd:YAG	Neodymium-doped yttrium aluminum garnet
NMR	Nuclear magnetic resonance spectroscopy
PhMgBr	Phenylmagnesium bromide
ppm	Parts per million
Q	Quadrupol

RF	Radio frequency
RTOF	Reflectron time-of-flight
SA	Sinapic acid
TCM	Chloroform
Th	Thomson
TOF	Time of flight
TTP	2,2':5',2''-Terthiophene
α-CHCA	α-Cyano-4-hydroxycinnamic acid

9 Bibliography

[1] W. C. Zeise, *Ann. Phys.* **1831**, *97*, 497–541.

[2] P. Ehrlich, A. Bertheim, *Berichte der Dtsch. Chem. Gesellschaft* **1912**, *45*, 756–766.

[3] H. J. NICHOLS, J. A. FORDYCE, *J. Am. Med. Assoc.* **1910**, *55*, 1171–1178.

[4] G. Cecchin, G. Morini, F. Piemontesi, in *Kirk-Othmer Encycl. Chem. Technol.*, American Cancer Society, **2003**.

[5] R. Colton, A. D'Agostino, J. C. Traeger, *Mass Spectrom. Rev.* **1995**, *14*, 79–106.

[6] G. A. Bailey, D. E. Fogg, *ACS Catal.* **2016**, *6*, 4962–4971.

[7] M. F. Wyatt, *J. Mass Spectrom.* **2011**, *46*, 712–719.

[8] G. Petroselli, M. K. Mandal, L. C. Chen, G. T. Ruiz, E. Wolcan, K. Hiraoka, H. Nonami, R. Erra-Balsells, *J. Mass Spectrom.* **2012**, *47*, 313–321.

[9] R. Cotton, Frank Albert and Wilkinson, Geoffrey and Murillo, Carlos A and Bochmann, Manfred and Grimes, *Advanced Inorganic Chemistry*, Wiley New York, **1988**.

[10] T. M. Trnka, R. H. Grubbs, *Acc. Chem. Res.* **2001**, *34*, 18–29.

[11] A. W. Prestayko, J. C. D'Aoust, B. F. Issell, S. T. Crooke, *Cancer Treat. Rev.* **1979**, *6*, 17–39.

[12] T. T. Tidwell, *Angew. Chemie Int. Ed.* **2001**, *40*, 331–337.

[13] E. de Hoffmann, in *Kirk-Othmer Encycl. Chem. Technol.*, American Cancer Society, **2005**.

[14] F. Hillenkamp, T. W. Jaskolla, M. Karas, in *MALDI MS*, John Wiley & Sons, Ltd,

2013, pp. 1–40.

[15] M. Yamashita, J. B. Fenn, *J. Phys. Chem.* **1984**, *88*, 4451–4459.

[16] J. B. Fenn, M. Mann, C. K. Meng, S. F. Wong, C. M. Whitehouse, *Science (80-.).* **1989**, *246*, 64 LP – 71.

[17] E. Pittenauer, N. S. Koulakiotis, A. Tsarbopoulos, G. Allmaier, *J. Mass Spectrom.* **2013**, *48*, 1299–1307.

[18] M. Karas, R. Krüger, *Chem. Rev.* **2003**, *103*, 427–440.

[19] M. Karas, D. Bachmann, U. Bahr, F. Hillenkamp, *Int. J. Mass Spectrom. Ion Process.* **1987**, *78*, 53–68.

[20] M. Karas, U. Bahr, F. Hillenkamp, *Int. J. Mass Spectrom. Ion Process.* **1989**, *92*, 231–242.

[21] E. De Hoffman, V. Stroobant, *Mass Spectrometry: Principles and Applications*, John Wiley & Sons, Ltd, **2007**.

[22] A. G. Marshall, C. L. Hendrickson, S. D.-H. Shi, *Anal. Chem.* **2002**, *74*, 252 A-259 A.

[23] *Zeitschrift für Naturforsch. A* **1953**, *8*, 448.

[24] W. C. Wiley, I. H. McLaren, *Rev. Sci. Instrum.* **1955**, *26*, 1150–1157.

[25] M. Kussmann, E. Nordhoff, H. Rahbek-Nielsen, S. Haebel, M. Rossel-Larsen, L. Jakobsen, J. Gobom, E. Mirgorodskaya, A. Kroll-Kristensen, L. Palm, et al., *J. Mass Spectrom.* **1997**, *32*, 593–601.

[26] M. Mastalir, M. Glatz, B. Stöger, M. Weil, E. Pittenauer, G. Allmaier, K. Kirchner, *Inorganica Chim. Acta* **2017**, *455*, 707–714.

[27] D. Benito-Garagorri, K. Kirchner, *Acc. Chem. Res.* **2008**, *41*, 201–213.

[28] M. Mastalir, B. Stöger, E. Pittenauer, M. Puchberger, G. Allmaier, K. Kirchner, *Adv. Synth. Catal.* **2016**, *358*, 3824–3831.

[29] K. Sládková, J. Houška, J. Havel, *Rapid Commun. Mass Spectrom.* **2009**, *23*, 3114–3118.

[30] "Bruker ultrafleXtreme MALDI-TOFMS," can be found under https://www.as.uky.edu/mass-spec-instrumentation#Bruker Ultraflextreme MALDI-TOFMS, **n.d.**

[31] Waters, *Synapt HDMS - The Science of What`s Possible*, **2007**.

[32] Agilent Technologies, *Agilent 6200 Series TOF and 6500 Series Q-TOF LC / MS System Concepts Guide_Sep15*, **2015**.